CASL-U-2018-1528-000

Verification and Validation of the ENDF/B-VII.1 v4.3m1 MPACT 51-Group Cross Section Library

Revision 0

Kang Seog Kim
Mark L. Williams
Dorothea Wiarda
Cole A. Gentry
Andrew T. Godfrey
Kevin T. Clarno
Oak Ridge National Laboratory

Yuxuan Liu
University of Michigan

Scott Palmtag
Core Physics

February 12, 2018

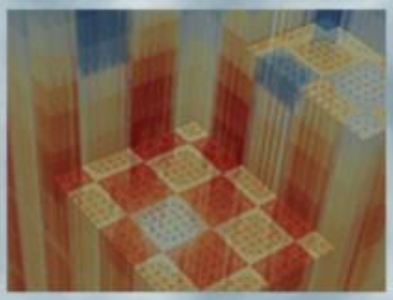

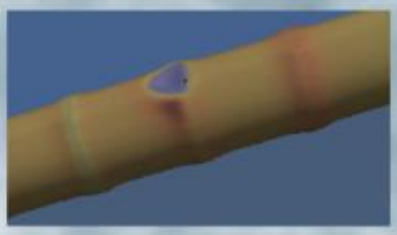

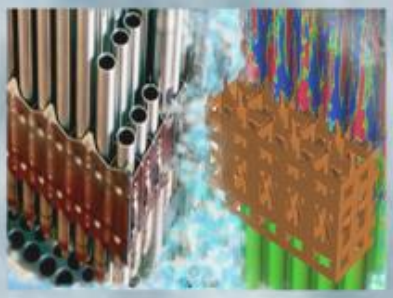

DOCUMENT AVAILABILITY

Reports produced after January 1, 1996, are generally available free via US Department of Energy (DOE) SciTech Connect.

Website www.osti.gov

Reports produced before January 1, 1996, may be purchased by members of the public from the following source:

National Technical Information Service
5285 Port Royal Road
Springfield, VA 22161
Telephone 703-605-6000 (1-800-553-6847)
TDD 703-487-4639
Fax 703-605-6900
E-mail info@ntis.gov
Website http://classic.ntis.gov/

Reports are available to DOE employees, DOE contractors, Energy Technology Data Exchange representatives, and International Nuclear Information System representatives from the following source:

Office of Scientific and Technical Information
PO Box 62
Oak Ridge, TN 37831
Telephone 865-576-8401
Fax 865-576-5728
E-mail reports@osti.gov
Website http://www.osti.gov/contact.html

REVISION LOG

Revision	Date	Affected Pages	Revision Description
0	2/12/2018	All	Initial version

Export Controlled None

IP/Proprietary/NDA Controlled None

Sensitive Controlled None

Unlimited All Pages

Requested Distribution:

To: N/A

Copy: N/A

Reviewed by:

Date:

Reviewer:

EXECUTIVE SUMMARY

The MPACT neutronics module of the Consortium for Advanced Simulation of Light Water Reactors (CASL) core simulator is a 3-D whole core transport code being developed for the Virtual Environment for Reactor Analysis (VERA) CASL toolset. Key characteristics of the MPACT code include (1) a subgroup method for resonance self-shielding and (2) a whole-core transport solver with a 2-D/1-D synthesis method. The MPACT code requires a cross section library to support all of its core simulation capabilities; a cross section library would be MPACT's most influencing component for simulation accuracy.

Due to the limitation of computing capacity even in high performance computing, the cross section library must be developed to enhance computational efficiency in memory and computing time without losing accuracy and generality. This requires a very coarse energy group structure with about 50 groups. Multigroup (MG) neutron cross section libraries for the CASL VERA-CS neutronics simulator MPACT have been created by using the AMPX/SCALE code package developed at Oak Ridge National Laboratory (ORNL).

A new 51-group structure was developed for efficient simulation to be applicable for both pressurized water reactor (PWR) and boiling water reactor (BWR) simulations. New v4.3m1 MPACT 51-group library with the ENDF/B- VII.1 nuclear data were developed for MPACT. Since SCALE KENO has some issues in the probability table and has a low cutoff energy for the free gas model, this issue has been corrected. This study focused on the development of the ENDF/B-VII.1 v4.3m1 MPACT MG library, including verification and validation.

This document includes the library generation methodology and procedure, the verification procedure, and benchmark results compared to continuous energy Monte Carlo results using newly developed cross section libraries.

TABLE OF CONTENTS

REVISION LOG iii

EXECUTIVE SUMMARY iv

FIGURES vii

TABLES ix

ACRONYMS x

1 INTRODUCTION 1

2 LIBRARY GENERATION METHODOLOGY AND PROCEDURE 2
2.1 MULTI-GROUP CROSS SECTION PROCESSING BY AMPX 2
2.2 IMPROVEMENT OF RESONANCE DATA 5
2.2.1 Intermediate Resonance (IR) Approximation and Parameters 5
2.2.2 Resonance Self-Shielded Data by Homogeneous Models 7
2.2.3 Resonance Self-Shielded Data by Heterogeneous Models 9
2.2.4 Self-shielded data for within-group elastic scattering 10
2.3 SUBGROUP DATA GENERATION 11
2.3.1 Subgroup method 11
2.3.2 Subgroup data generation 13
2.3.3 Subgroup method for nonuniform temperature distribution 15
2.4 TRANSPORT CROSS SECTIONS FOR ^{1}H 16
2.5 SPH METHOD FOR THE ^{238}U SUBGROUP DATA 18

3 THE IMPACT 51-GROUP LIBRARY GENERATION 21
3.1 AMPX 51-GROUP LIBRARY 21
3.2 MPACT 51-GROUP LIBRARY 22

4 VERIFICATION AND VALIDATION 25
4.1 VERA CORE PHYSICS BENCHMARK PROGRESSION PROBLEMS 25
4.1.1 Characteristics of Benchmark Problems 25
4.1.2 Benchmark Results 26
4.2 EXTENDED VERA BENCHMARK PROGRESSION PROBLEMS 29
4.2.1 Characteristics of Problems 29
4.2.2 Benchmark Results 29
4.3 VERA Depletion Benchmark Problems 31
4.3.1 Characteristics of Problems 31
4.3.2 Benchmark Results 32
4.4 EXTENSIVE PWR PIN AND ASSEMBLY BENCHMARK PROBLEMS 38
4.4.1 Characteristics of Problems 38
4.4.2 Benchmark Results 40
4.5 NONUNIFORM FUEL TEMPERATURE BENCHMARK PROBLEMS 48
4.5.1 Characteristics of Problems 48
4.5.2 Benchmark Results 49

4.6 MOSTELLER BENCHMARK PROBLEMS 52
4.6.1 Characteristics of Problems 52
4.6.2 Benchmark Results 52

5 CONCLUSIONS AND FUTURE WORK 55

REFERENCES 56

FIGURES

Figure 2.1. AMPX/SCALE Procedure to Generate the AMPX MG Library. 2
Figure 2.2. Pointwise Neutron Spectra Obtained by CENTRM. 5
Figure 2.3. Resonances and Subgroups. 11
Figure 2.4 Resonance Data Generation Procedure. 14
Figure 2.5. 51-Group Transport Correction Factors for ^{1}H. 18
Figure 2.6. SPH Method to Generate the ^{238}U Subgroup Data. 19
Figure 2.7. ^{238}U 51-Group Absorption Reaction Rate Differences with/without SPH Factors. 20
Figure 3.1. DECLIB Calculation Flow. 24
Figure 4.1. Problem 2 lattice Layouts (Octant Symmetry). 26
Figure 4.2. Pin Power Comparisons for Problem 5A-2D. 28
Figure 4.3. Comparison of Simplified Burnup Chain to Full Burnup Chain. 33
Figure 4.4. Comparison of Multiplication Factors between KENO and MPACT P_2 with Epithermal Upscattering. 34
Figure 4.5. Comparison of Multiplication Factors between KENO and MPACT TCP_0 with Epithermal Upscattering. 34
Figure 4.6. Comparison of Pin Powers between KENO and MPACT P_2 with Epithermal Upscattering. 35
Figure 4.7. Comparison of Multiplication Factors between KENO and MPACT P_2 without Epithermal Upscattering. 35
Figure 4.8. Comparison of Multiplication Factors between KENO and MPACT P_2 without Epithermal Upscattering. 36
Figure 4.9. Comparison of Pin Powers between KENO and MPACT P_2 without Epithermal Upscattering. 36
Figure 4.10. Comparison of Multiplication Factors between ENDF/B-VII.0 and ENDF/B-VII.1 using SERPENT without Epithermal Upscattering. 37
Figure 4.11. Pin k_{eff} Difference Distribution with Epithermal Upscattering. 43
Figure 4.12. Pin k_{eff} Difference Distribution without Epithermal Upscattering. 43
Figure 4.13. Assembly k_{eff} Difference Distribution with Epithermal Upscattering. 47
Figure 4.14. Assembly k_{eff} Difference Distribution without Epithermal Upscattering. 47
Figure 4.15. Geometrical Configuration. 49
Figure 4.16. Comparison of Reactivities between Nonuniform and Uniform Temperature Distributions. (KENO). 50

Figure 4.17. Comparison of Reactivities for the Uniform Temperature Distributions. 51
Figure 4.18. Comparison of Reactivities for the Nonuniform Temperature Distributions. 51
Figure 4.19. Comparison of Reactivities for the Nonuniform Temperature Distributions with Epithermal Upscattering. 54
Figure 4.20 Comparison of Reactivities for the Nonuniform Temperature Distributions without Epithermal Upscattering. 54

TABLES

Table 2.1. Variations for ^{238}U for the Heterogeneous Models 10
Table 3.1. The 51-Group Structure 21
Table 3.2 List of Nuclides, Including Subgroup Data 22
Table 4.1. Details of the VERA Progression Problems 25
Table 4.2. Results with the ENDF/B-7.1 MPACT 51-g Library 27
Table 4.3. Results for 2D Core Problems with the ENDF/B-7.1 Library. 28
Table 4.4. Extended VERA Benchmark Problems 29
Table 4.5. Benchmark Result with the ENDF/B-7.1 MPACT 51-g Library 30
Table 4.6. Single Pin and Assembly Depletion Benchmark Problems 31
Table 4.7. Moderator Temperatures and Densities 38
Table 4.8. Pin Cell Dimensions 38
Table 4.9. Assembly Geometry Descriptions 39
Table 4.10. Assembly dimensions 40
Table 4.11. Benchmark Result for Pin Cell Problems (P_2) 41
Table 4.12. Benchmark Result for Pin Cell Problems (TCP_0) 42
Table 4.13 Benchmark Result for Assembly Problems with Epithermal Upscattering 45
Table 4.14 Benchmark Result for Assembly Problems without Epithermal Upscattering 46
Table 4.15. Geometrical Data 48
Table 4.16. Composition Data 48
Table 4.17. Nonuniform Temperature Profiles as a Function Power 49
Table 4.18. Atomic Number Densities of UO_2 Fuels 52
Table 4.19. Geometrical Configurations 52
Table 4.20. Atomic Number Densities of Moderator and Clad 52
Table 4.21. Benchmark Results for Mosteller 53
Table 5.1. v4.3m1 MPACT 51-Group Library 55

ACRONYMS

AMPX	resonance processing code; the name is no longer an acronym
ANS	American Nuclear Society
CASL	Consortium for Advanced Simulation of Light Water Reactors
CE	continuous energy (as in cross sections)
CENTRM	PW transport code in SCALE
CMFD	coarse-mesh finite difference
CTF	COBRA TF
DBRC	Doppler broadening rejection correction
ENDF	evaluated nuclear data file
ESSM	embedded self-shielding method
GT	guide tube
IFBA	integral fuel burnable absorber
IR	intermediate resonance
IT	instrument tube
KERMA	kinetic energy released per unit mass
LWR	light-water reactor
MCNP	Monte Carlo N-Particle
MG	multigroup (as in cross sections)
MPACT	radiation transport code in VERA; the name is no longer an acronym
NJOY	nuclear data code
NLC	neutron leakage conversion
NR	narrow resonance
ORIGEN	Oak Ridge Isotopic Generation code in SCALE
ORNL	Oak Ridge National Laboratory
PW	pointwise
PWR	pressurized water reactor
RI	resonance integral
RIA	reactivity insertion accident
SAMPX	simplified AMPX
SCALE	Standardized Computer Analyses for Licensing Evaluations code
SNU	Seoul National University
SPH	super-homogenization
SQA	software quality assurance
T/H	thermal/hydraulic
URR	unresolved resonance
VERA	Virtual Environment for Reactor Applications
VERA-CS	VERA Core Simulator
WR	wide resonance
XS	cross section

1 INTRODUCTION

The MPACT [Mpa13] neutronics module of the Consortium for Advanced Simulation of Light Water Reactors (CASL) [CAS15] core simulator is a 3-D whole core transport code being developed for the CASL toolset, Virtual Environment for Reactor Analysis (VERA) [Tur16]. MPACT is under development for neutronics simulation coupled with the COBRA-TF (CTF) code for thermal-hydraulics simulation for pressurized light water reactors (LWRs). Key characteristics of the MPACT code include (1) a subgroup method for resonance self-shielding and (2) a whole-core transport solver with a 2-D/1-D synthesis method. Thus, the MPACT code requires a cross section library to support all the MPACT core simulation capabilities.

Multigroup (MG) neutron cross section libraries for the CASL MPACT neutronics code [Mpa13], which is part of the VERA core simulator, have been developed by using the AMPX code package [Wia16] and the XSTools software in VERA. The native MPACT cross section library format, which is based on the HELIOS [Sta98] and DeCART [Cho02] formats, is the primary structure available for CASL. The ^{238}U resonance self-shielded cross section tables have been developed based on SCALE KENO, by which the super-homogenization (SPH) factors have been obtained. KENO has had several issues, including probability table and a low cutoff energy for the free gas mode. Since the KENO issues have been resolved, new ^{238}U SPH factors have been estimated and used to generate the ^{238}U resonance cross section tables. The fuel temperature reactivity bias still needs to be resolved. MPACT is required to deliver verified and validated MPACT MG cross section libraries based on the CASL Software Quality Assurance (SQA) procedure.

This document includes the following:

- The library generation procedure, including the methodology and verification (Chapter 3),
- Generation of the v4.3m1 MPACT 51-g library with ENDF/B-VII.1 (Chapter 4), and
- Benchmark calculations and results (Chapter 5),

This study is a part of verification and validation for CASL VERA's MG cross section library.

2 LIBRARY GENERATION METHODOLOGY AND PROCEDURE

The VERA neutronics simulator MPACT requires MG neutron cross section data to solve the Boltzmann transport equation in order to obtain neutron flux distribution. The evaluated nuclear data files (ENDF/B) are processed to generate MG cross sections by using the AMPX-6 [Wia16] and SCALE [Sca16] code packages developed at Oak Ridge National Laboratory (ORNL). The MPACT MG library is generated by using the CASL XSTools [Kim15] with the AMPX MG master library and other nuclear data. Figure 2.1 illustrates the AMPX/SCALE procedure to generate the AMPX MG library, where the left side of flow chart shows the conventional procedure, and the right side illustrates the new procedure to improve the Bondarenko resonance data. This section summarizes the methodology and procedure to prepare the VERA MPACT MG cross section library.

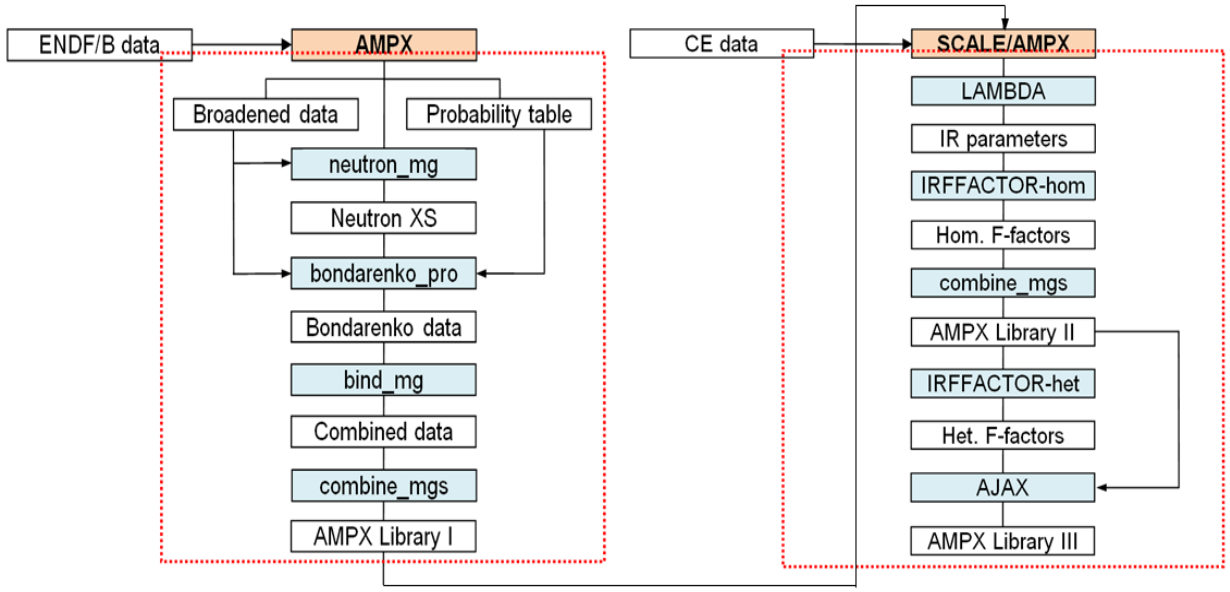

Figure 2.1. AMPX/SCALE Procedure to Generate the AMPX MG Library.

2.1 MULTI-GROUP CROSS SECTION PROCESSING BY AMPX

AMPX-6 [Wia16] is a modular system of FORTRAN computer programs that is used to generate the MG and continuous energy (CE) cross section libraries for modern deterministic and Monte Carlo transport codes by processing ENDF/B libraries. Since the CASL neutronics simulator MPACT is a deterministic transport code, only the AMPX MG library generation procedure is discussed here.

The AMPX MG library includes various neutron reactions of the Bondarenko F-factors, which are defined as ratios of resonance self-shielded cross sections to infinite dilution cross sections as a function of background cross sections for all energy groups, including resolved and unresolved resonances. The resolved resonance F-factors have

been generated by the narrow resonance (NR) approximation, and the unresolved resonance F-factors have been generated by the probability table method based on the NR approximation [Cul74, Kim18]. MG cross sections and scattering matrices were obtained by using a weighting function of Maxwellian spectrum + 1/E + fission spectrum. At low energies, the weighting function is a Maxwellian spectrum which has a flux shape that assumes the neutron scatters into a region with a free gas scatterer with no absorption. The Maxwellian flux spectrum has the following formula:

$$\phi(E) = M(E) = Ee^{-\frac{E}{kT}}, \tag{2.1}$$

where *E* denotes neutron energy, *k denotes the* Boltzmann constant, and *T* denotes temperature of the material in Kelvin. In the slowing down range, 0.125 eV < *E* < E_{cut}, the weighting spectrum is assumed to be $\phi(E) = 1/E$. The cutoff energy E_{cut} for the slowing down range must be selected and is typically 55 keV by default in the AMPX modules. In the region E_{cut} < *E* < 10^7 eV, where fission neutrons are born, the following fission spectrum is used.

$$f(E) = c(E) = E^{0.5}e^{-\frac{E}{q}}, \tag{2.2}$$

where θ is temperature of the fission spectrum (e.g., 1.2 × 10^6 eV). For energies above 10^7 eV, the particles are considered to be in another slowing down region, so the spectrum is assumed to have a *1/E* shape.

MG self-shielded cross sections of reaction type *i* (Bondarenko F-factors) as a function of background cross sections (σ_0) and material temperature (*T*) are calculated by using the following equation based on NR approximation:

$$\sigma_{i,g}(T,\sigma_0) = \frac{\int_g \frac{\sigma_i(T,E)\sigma_0\phi(E)}{\sigma_t(T,E)+\sigma_0}dE}{\int_g \frac{\sigma_0\phi(E)}{\sigma_t(T,E)+\sigma_0}dE}, \tag{2.3}$$

where T denotes temperature, and σ_t is total cross section. The MG scattering matrix can be obtained by

$$\sigma_{s,l,gg'} = \frac{1}{\int_g \phi(E)dE}\int_g y(E)\sigma_s(E)\phi(E)dE\int_{g'} f_l(E,E')dE', \tag{2.4}$$

where $y(E)$ is a multiplicity which is unity for scattering, and $f_l(E,E')$ is a normalized double differential distribution. It should be noted that the scattering matrix data (not for thermal scattering matrices) are temperature-independent in the AMPX MG library.

Typically, NR approximation could be a good solution for the unresolved resonance (URR) energy range in which pointwise (PW) neutron spectrum could be approximated in terms of total and background cross sections. Since the probability tables are provided at the URR energy range, including cross section levels and weights, MG self-shielded cross section tables (F-factor tables) could be obtained by using an NR approximation with a probability table, as follows:

$$\sigma_{x,g}(\sigma_0) = \frac{\int_g \sum_m p^m \sigma_x^m(E)\phi^m(E,\sigma_0)dE}{\int_g \sum_m p^m \phi^m(E,\sigma_0)dE}, \tag{2.5}$$

$$\varphi^m(E,\sigma_0) = \frac{\sigma_0}{\sigma_t^m(E)+\sigma_0}\phi(E), \tag{2.6}$$

where

σ_0 = background cross section,
σ_x^m = a cross section level of the level *m* and reaction *x*,
σ_t^m = a total cross section level of the level *m*,
p^m = a probability of the level *m*, and
$\sigma_{x,g}$ = a self-shielded cross section of reaction *x*.

In the standard SCALE sequences (e.g., TRITON), self-shielded MG cross sections and scattering matrices for resolved resonance and thermal energy groups are determined by performing the problem-dependent CENTRM slowing down transport calculation for each pin cell type with Eq. (2.7). Therefore, the resolved resonance data in the AMPX MG library are not used.

$$\hat{\Omega}\cdot\nabla\psi + \Sigma_t(\vec{r},u)\psi(\vec{r},u,\hat{\Omega}) = \int_{4\pi} d\Omega' \int_0^\infty du' \Sigma_s(\vec{r},u'\to u,\hat{\Omega}'\cdot\hat{\Omega})\psi(\vec{r},u',\hat{\Omega}') + q(\vec{r},u,\hat{\Omega}), \tag{2.7}$$

where

$\hat{\Omega}$ = neutron direction,
$\vec{r}$ = space coordinate,
u = neutron lethargy,
ψ = angular flux,
Σ_t = macroscopic total cross section,
Σ_s = double differential scattering cross section, and
q = external source.

However, since the Bondarenko approach for the resonance self-shielding calculation does not include any problem-dependent PW slowing down calculations, a weighting function would make a significant impact on the accuracy, mostly through the scattering matrix. The weighting function of Maxwellian spectrum + 1/E + fission spectrum is far from realistic. Practical weighting functions for various temperatures can be obtained by performing the CENTRM MG/PW calculations for a typical PWR fuel pin. Figure 2.2

provides a sample of PW neutron spectra obtained by CENTRM. This would be performed using the XSProc sequence with “parm=centrm”; the weight functions must be generated to include various temperatures.

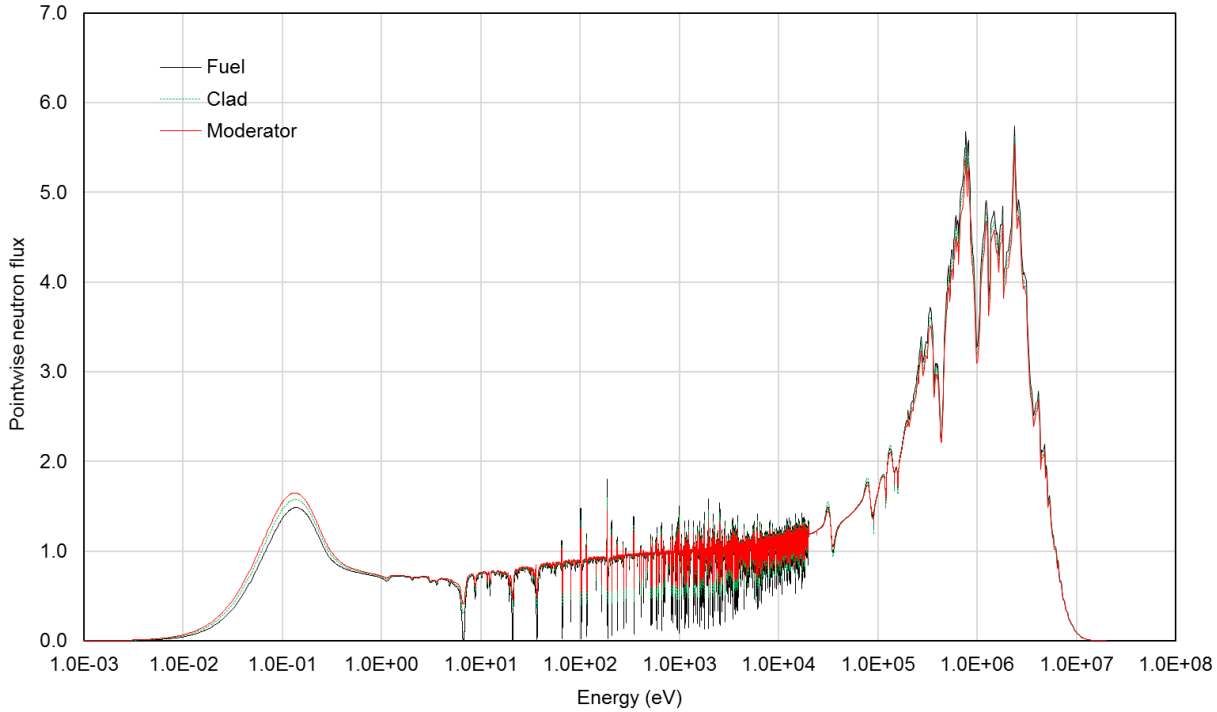

Figure 2.2. Pointwise Neutron Spectra Obtained by CENTRM.

There is a pending issue associated with the PW weighting function in the Bondarenko approach. Since resonance self-shielded cross sections are independently estimated, they are independent of the PW weighting function. In reality, since the current MPACT procedure includes resonance data only for the specified energy groups, self-shielded cross sections of nonresonance groups should be dependent on the weighting functions. MG scattering matrices are obtained by simple P_0 flux moment weighting, and renormalization is applied only to total scattering, within-group, and out-scattering components. Therefore, this procedure may introduce incorrect neutron fluxes, resulting in some errors in reaction rates. PW neutron spectra are very changeable according to ^{235}U enrichment, moderator-to-fuel ratio, burnup, and void fraction. Therefore, selecting the weighting function would be challenging.

2.2 IMPROVEMENT OF RESONANCE DATA

2.2.1 Intermediate Resonance (IR) Approximation and Parameters

To cast the scattering source term into a more tractable form, the intermediate resonance (IR) approximation is introduced. In this approximation, the fraction λ_i of the scattering for each isotope *i* is assumed to be so effective that the maximum lethargy gain per collision is significantly greater than the practical resonance width (i.e., the NR

scattering) [Sta83, Sta03]. A resonance affects only a small interval of the integration range from u-Δ_i to u, and its contribution to the scattering source $Q(u)$ is negligible. Outside the resonances, $\Sigma_{si}(u)=\Sigma_{pi}$ and $\phi(u)=constant$, so the contribution of isotope i to $Q(u)$ is $\lambda_i\Sigma_{pi}$. This is the unperturbed slowing down source. Conversely, the remaining fraction (1-λ_i) is assumed to be so ineffective that neutrons gain a negligible amount of lethargy compared with Δu_g (i.e., the wide resonance [WR] scattering). The resonances are so wide that the integrand can be replaced by its average value, which leads to the $(1-\lambda_i)\Sigma_{si}(u)\phi(u)$ contribution to the source $Q(u)$. Thus, this fraction of scattering does not provide source neutrons from outside the resonance widths, but it should be considered as a result of self-scattering, which neither adds nor removes neutrons. With these approximations, Eq. (2.7) can be rewritten for the coarse energy groups:

$$\hat{\Omega}\cdot\nabla\psi_{g,k}+\sum_i\Sigma^k_{i,g,t}\psi_{g,k}(\hat{\Omega})=\sum_i\lambda_{i,g}\Sigma^k_{i,p}+\sum_i(1-\lambda_{i,g})\Sigma^k_{i,g,s}\phi_{g,k}. \tag{2.8}$$

Eq. (2.8) can be rewritten by assuming isotropic angular flux and $\Sigma_{i,p}=\Sigma_{i,g,s}$ as

$$\hat{\Omega}\cdot\nabla\psi_{g,k}+\sum_i(\Sigma^k_{i,g,a}+\lambda_{i,g}\Sigma^k_{i,p})\psi_{g,k}(\hat{\Omega})=\sum_i\lambda_{i,g}\Sigma^k_{i,p}. \tag{2.9}$$

For the homogeneous mixture, the self-shielded flux can be obtained from Eq. (2.9) as

$$\phi_g=\frac{\sum_i\lambda_{i,g}\Sigma_{i,p}}{\sum_{i=resonance}\Sigma_{i,g,a}+\sum_i\lambda_{i,g}\Sigma_{i,g,s}}=\frac{\lambda_g\Sigma_p}{\Sigma_{g,a}+\lambda_g\Sigma_{g,s}}. \tag{2.10}$$

The IR parameter [Gol62] can be defined as a probability passing through resonance without any reaction, which correlates the NR and WR approximations. Since the atomic mass of hydrogen (^{1}H) is very close to unity, the lethargy gain of any neutron colliding with hydrogen is very large, and the neutron can scatter beyond a resonance without any collision. This is essentially the same as the NR approximation. Therefore, for hydrogen, the IR parameter is defined as unity. For other nuclides, the IR parameter is obtained by comparing results of various ^{238}U/^{1}H mixtures where the hydrogen is partly replaced by the other isotopes [Les87]. This is often referred to as a *hydrogen-equivalence parameter*.

First, a self-shielded cross section table, $\sigma^{238}_{g,a}$ vs. $\sigma^{238}_{g,b}$, must be prepared by performing slowing down calculations with various hydrogen atomic number densities (N^1) with a fixed ^{238}U atomic number density (N^{238}). The background cross sections can be obtained using the following equation, assuming the ^{1}H (λ^1_g) and ^{238}U (λ^{238}_g) IR parameters to be unity.

$$\sigma^{238}_{g,b}=\frac{N^{238}\lambda^{238}_g\sigma^{238}_p+N^1\lambda^1_g\sigma^1_p}{N^{238}}=\frac{\sum_{i=all}N^i\lambda^i_g\sigma^i_p}{N^R}. \tag{2.11}$$

Then the slowing down calculation is performed for a mixture of ^{238}U, ^{1}H and a target nuclide *x*. A new $\sigma_{g,a}^{238}$ is calculated, and the corresponding $\sigma_{g,b}^{238}$ is read from the prepared $\sigma_{g,a}^{238}$ table. The IR parameter (λ_g^x) for a nuclide *x* can be obtained by using Eq. (2.12),

$$\lambda_g^x = \frac{\sigma_{g,b}^{238} N^{238} - N^{238}\lambda_g^{238}\sigma_p^{238} - N^1\lambda_g^1\sigma_p^1}{N^x\sigma_p^x}, \tag{2.12}$$

where σ_p^x is the potential cross section. The IR parameter of ^{238}U should be determined first, and then the IR parameters of other nuclides should be evaluated. The LAMBDA program shown in Figure 2.1 computes all of the IR parameters for all nuclides by using this procedure.

2.2.2 Resonance Self-Shielded Data by Homogeneous Models

The energy dependence of the cross sections in the library has been discretized by dividing the energy range of interest, 10^{-5}eV–20MeV, into a number of broad groups. These cross sections have been obtained by flux-averaging PW cross sections—sometimes more than 10^5 points with typical reactor spectra. However, this procedure is impractical for the resonance isotopes in the range from 100KeV–1eV. In this range, the cross sections exhibit many resonances, so thousands of energy groups would be required for a satisfactory discretization. In general, the number of resonance groups is limited to 5–30 for very coarse group structures including 50–60 energy groups, though SCALE generally uses well over 250 energy groups. The objective of the resonance treatment is to evaluate the effective cross section for the resonance isotopes in all resonance energy groups:

$$\sigma_{x,g} = \frac{\int_{\Delta u_g} \sigma_x(u)\phi(u)du}{\int_{\Delta u_g} \phi(u)du}. \tag{2.13}$$

In Eq. (2.13), the lethargy ($u=ln(E_0/E)$, E_0=10MeV) is used instead of the neutron energy, and *x* represents a reaction type. However, the library data available for this purpose are in tables of group-dependent resonance integrals (RIs), or the numerator of Eq. (2.13) vs temperatures and background cross sections. In CENTRM, the flux in Eq. (2.13) is calculated by solving the neutron slowing down equation for homogeneous or heterogeneous system.

To describe the slowing down equation in a homogeneous infinite system containing a mixture of isotopes, indexed *i*, of which one is a resonance absorber, the following three assumptions are used:

a. Nonresonance isotopes have negligible absorption and a constant potential scattering cross section for the resonance energy range.

b. Resonance isotopes have resonance absorption cross sections as represented by $\sigma_{ai}(u)$, and scattering cross sections as represented by $\sigma_{rs,i}(u)$, in addition to the potential scattering cross section, σ_{pi}. However, apart from the resonance energy region, these resonance absorption and scattering cross sections are negligible.
c. The resonances are so well separated that the flux between them has its constant asymptotic value, as it is set to 1.

With these assumptions, the slowing down equation at the resonance energy region, away from fission sources, is given by

$$\begin{aligned} &\Sigma(u)\phi(u) = Q(u), \\ &Q(u) = \sum_i \int_{u-\Delta_i}^{u} \Sigma_{si}(u')\phi(u')\frac{\exp(u'-u)}{1-\alpha_i}du', \end{aligned} \tag{2.14}$$

where

$$\begin{aligned} &\Sigma_{xi} = N_i\sigma_{xi}, \\ &\Sigma_{si}(u) = \Sigma_{pi} + \Sigma_{rs,i}(u), \\ &\Sigma_i(u) = \Sigma_{si}(u) + \Sigma_{ai}(u), \\ &\Sigma(u) = \sum_i \Sigma_i(u), \\ &\alpha_i = (A_i-1)^2/(A_i+1)^2, \\ &\Delta_i = -\ln(\alpha_i). \end{aligned} \tag{2.15}$$

In Eq. (2.15), $\Sigma(u)$ is the total macroscopic cross section, and N is atomic number density, while A_i is the atomic mass, and Δ_i is the maximum lethargy gain per collision with isotope i. $1-\alpha_i$ is the maximum fractional energy loss per collision with isotope i.

In a homogeneous system, for a given composition, the self-shielded cross section can be calculated using Eqs. (2.13) through (2.15), and the corresponding background cross section can be calculated using Eq. (2.16).

$$\sigma_b = \frac{\sum_{i=all} N_i\lambda_i\sigma_{i,p}}{N_R}. \tag{2.16}$$

Different background cross sections can be obtained by using various composition mixtures, typically a mixture of ^{1}H and a target resonance nuclide, creating a self-shielded cross section table as a function of background cross section. Therefore, for a given composition, the corresponding background cross section can be easily calculated using Eq. (2.16), and the self-shielded cross section can be read from the table directly.

2.2.3 Resonance Self-Shielded Data by Heterogeneous Models

In a heterogeneous system, for a given composition and geometry, the self-shielded cross section can also be calculated using Eqs. (2.13) through (2.15). However, since there is a leakage effect in Eq. (2.7), Eq. (2.13) cannot be used to obtain the corresponding background cross section. Therefore, the equivalence theory between the infinite homogeneous and heterogeneous problems was devised by introducing an equivalence cross section (Σ_e), as follows:

$$\Sigma_b = \lambda\Sigma_p \quad \rightarrow \quad \Sigma_b = \lambda\Sigma_p + \Sigma_e . \tag{2.17}$$

Thus, the balance equation with an equivalence theory and an elimination of the scattering resonance ($\lambda\Sigma_{rs}$) becomes:

$$(\Sigma_a + \lambda\Sigma_p + \Sigma_e)\phi = \lambda\Sigma_p + \Sigma_e . \tag{2.18}$$

The background cross section is not a physical quantity, but an artificial one used to retrieve the correct self-shielded cross section at a given composition and geometry. It is only important to be consistent in the procedures between its generation and its use. Therefore, the elimination of the scattering resonance is possible as long as consistency is maintained. In a heterogeneous system, the self-shielded scalar flux can be obtained by solving Eq. (2.8) with a self-shielded absorption cross section obtained by solving Eq. (2.7). The corresponding background cross section is obtained as follows:

$$\sigma_{g,b} = \frac{\Sigma_{g,b}}{N_R} = \frac{\sum_i N_i \lambda_i \sigma_{i,g,p} + \Sigma_{g,e}}{N_R} = \frac{\sigma_{g,a}\phi_g}{1-\phi_g} . \tag{2.19}$$

The following is a procedure to obtain the self-shielded cross section table by using the heterogeneous models.

a. Compute the PW slowing down calculations with Eq. (2.7) by using CENTRM for the heterogeneous models.
b. Edit various MG self-shielded cross sections for various reactions, including capture ($\sigma_{g,a}$), fission ($\sigma_{g,f}$), elastic scattering ($\sigma_{g,s}$) and within-group elastic scattering, using Eq. (2.13).
c. Solve the MG fixed source Eq. (2.8) or (2.9), which is called the *embedded self-shielding method* (ESSM) [Wil12] equation, with $\sigma_{g,a}$ from step b to obtain the scalar flux (ϕ_g).
d. Obtain the corresponding background cross section *($\sigma_{g,b}$)* using Eq. (2.19) for the heterogeneous model.
e. Repeat steps a–d, changing the geometry and composition configurations to obtain different background cross sections.
f. Complete the self-shielded cross section tables as a function of background cross section for various reactions.
g. Repeat the above procedures for various temperatures.

Various background cross sections can be achieved by changing geometrical and compositional configurations, as shown in Table 2.1.

Table 2.1. Variations for ^{238}U for the Heterogeneous Models

Case		1	2	3	4	5	6	7	8	9	10	11	12	13	14	15	16	17	18	19
Volume	Fuel	1	1	1	1	1	1	1	1	1	1	1	1	1	1	1	1	1	1	1
	Clad	1	1	1	1	1	1	1	1	1	1	1	1	1	1	1	1	1	1	1
	Mod	1	1	1	1	1	2	5	5	5	5	5	5	5	5	5	5	5	5	5
Fuel	^{235}U	1	1	1	1	1	1	1	$\frac{1}{2}$	$\frac{1}{4}$	$\frac{1}{8}$	$\frac{1}{16}$	$\frac{1}{32}$	$\frac{1}{10^2}$	$\frac{1}{10^2}$	$\frac{1}{10^2}$	$\frac{1}{10^2}$	$\frac{1}{10^2}$	$\frac{1}{10^2}$	$\frac{1}{10^2}$
	^{238}U	1	1	1	1	1	1	1	$\frac{1}{2}$	$\frac{1}{4}$	$\frac{1}{8}$	$\frac{1}{16}$	$\frac{1}{32}$	$\frac{1}{10^2}$	$\frac{3}{10^3}$	$\frac{1}{10^3}$	$\frac{1}{10^4}$	$\frac{1}{10^5}$	$\frac{1}{10^7}$	$\frac{1}{10^8}$
	^{16}O	1	1	1	1	1	1	1	$\frac{1}{2}$	$\frac{1}{4}$	$\frac{1}{8}$	$\frac{1}{16}$	$\frac{1}{32}$	$\frac{1}{10^2}$	$\frac{1}{10^2}$	$\frac{1}{10^2}$	$\frac{1}{10^2}$	$\frac{1}{10^2}$	$\frac{1}{10^2}$	$\frac{1}{10^2}$
H_2O	^{1}H	$\frac{1}{400}$	0.2	0.5	0.75	1	1	1	1	1	1	1	1	1	1	1	1	1	1	1
	^{16}O	$\frac{1}{400}$	0.2	0.5	0.75	1	1	1	1	1	1	1	1	1	1	1	1	1	1	1

In Eq. (2.13), the numerator is defined as an RI with the flux and cross section. In Stamm'ler and Abbate's work [Sta83], the self-shield cross section is approximated using the background cross section and the RI:

$$\sigma_{g,a}(\sigma_b) = \frac{R_{g,a}(\sigma_b)}{1 - R_{g,a}(\sigma_b)/\sigma_b}, \tag{2.20}$$

and

$$\nu\sigma_{g,f}(\sigma_b) = \frac{R_{g,\nu f}(\sigma_b)}{1 - R_{g,a}(\sigma_b)/\sigma_b}, \tag{2.21}$$

where ν is the number of neutrons released from a fission, and $R_{g,a}$ and $R_{g,\nu f}$ are absorption and ν*fission RIs, respectively. Using Eqs. (2.20) and (2.21), the self-shield cross section table can be converted into the RI table.

2.2.4 Self-shielded data for within-group elastic scattering

The AMPX MG library does not include a temperature-dependent elastic scattering matrix, which results in temperature bias when performing self-shielding calculation based on Bondarenko approach. Recently, a new MT=2022 has been added to consider removal correction to generate a temperature-dependent elastic scattering matrix. The new MT=2022 is for the within-group cross section (σ_g^{within}) for elastic scattering, which includes resonance self-shielded cross section tables. If the background cross section is determined by the ESSM or subgroup method, then the total elastic and within-group elastic cross sections can be obtained through

interpolation. The temperature-dependent elastic scattering matrix at temperature *T* can be obtained by using the following equations:

$$\tilde{\sigma}_{gg}^{elastic}(T) = \sigma_{g}^{within}(T)\,. \tag{2.22}$$

$$\tilde{\sigma}_{gg'}^{elastic}(T) = \sigma_{gg'}^{elastic}(T_0)\cdot\frac{\sigma_{g}^{elastic}(T)-\sigma_{g}^{within}(T)}{\sum_{g'}\sigma_{gg'}^{elastic}(T_0)-\sigma_{gg}^{elastic}(T_0)}\,. \tag{2.23}$$

2.3 SUBGROUP DATA GENERATION

2.3.1 Subgroup method

Figure 2.4 shows the coarse energy group, including resonances. An effective self-shielded cross section for this group can be obtained by the following flux weighting using Eq. (2.13). In the subgroup method, the resonances are divided by the subgroup levels, and the corresponding probability for each subgroup level (σ_{xn}) is defined as the subgroup weight (w_{xn}), as shown in Figure 2.4. [Sta03] Therefore, Eq. (2.13) can be approximated with removing the coarse group index, as follows:

$$\sigma_x = \frac{\sum_n w_{xn}\sigma_{xn}\phi_n}{\sum_n w_{an}\phi_n}\,, \tag{2.24}$$

where the summation of the subgroup weights is unity.

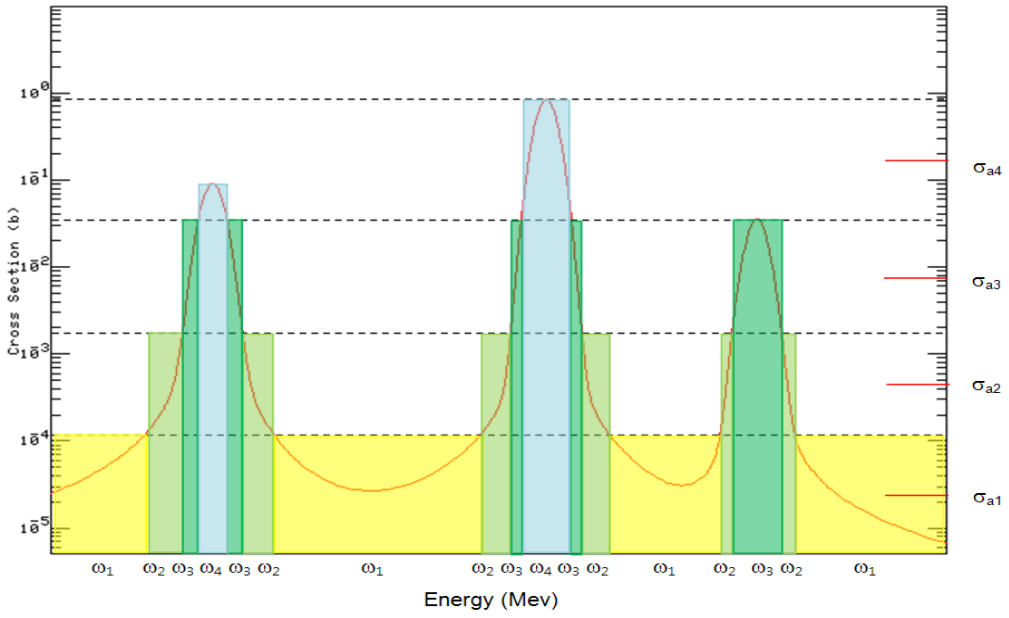

Figure 2.3. Resonances and Subgroups.

In the transport calculation, the final goal of the resonance treatment is to construct a procedure so that the self-shielded cross section estimated by Eq. (2.24) will be identical to the self-shielded cross section by Eq. (2.13). The self-shielded scalar flux ϕ_n in Eq. (2.26) should be estimated from the fixed source transport calculation. If there is only one resonant nuclide, the fixed source transport equation will be

$$\hat{\Omega}\cdot\nabla\psi_n + (N_r\sigma_{an} + \sum_i \lambda_i \Sigma_p^i)\psi_n = \sum_i \lambda_i \Sigma_p^i \,, \tag{2.25}$$

and

$$\phi_n = \int \psi_n d\hat{\Omega} \,, \tag{2.26}$$

where N_r denotes the particle number density for the resonant nuclide, Σ_p is a potential cross section, and ψ_n is an angular flux. Equivalence theory enforces that the self-shielded scalar flux is expressed with the absorption (σ_{an}) and the background cross sections (σ_{bn}).

$$\phi_n = \frac{\sigma_{bn}}{\sigma_{an} + \sigma_{bn}} \,. \tag{2.27}$$

Typically, the background cross section in the heterogeneous model is divided into two parts.

$$\sigma_{bn} = \lambda\sigma_p + \sigma_{en}(\sigma_{an}) \,, \tag{2.28}$$

where λ denotes an intermediate resonance parameter, σ_p is a potential cross section, and σ_{en} is an equivalence cross section. By using Eq. (2.27), Eq. (2.24) can be written as follows:

$$\sigma_x = \frac{\sum_n w_{xn}\sigma_{xn}\dfrac{\sigma_{bn}}{\sigma_{an}+\sigma_{bn}}}{1-\sum_n w_{an}\dfrac{\sigma_{an}}{\sigma_{an}+\sigma_{bn}}} \,. \tag{2.29}$$

Therefore, if the subgroup levels and weights are given for a certain nuclide, the effective self-shielded cross section can be obtained by estimating the corresponding background cross sections (σ_{bn}) in the lattice calculation. Since the equivalence cross section is not sensitive to the absorption cross section but is sensitive to the geometrical configuration, σ_{bn} is often approximated by a single background cross section σ_b. If there are several resonant nuclides, there will be a resonant interference between the resonant nuclides. Since this interference will have an effect on the self-shielded scalar flux, Eq. (2.29) can be written as follows:

$$\sigma_x = \frac{\sum_n w_{xn}\sigma_{xn}\dfrac{\sigma_{bn}}{\sigma_{an}+\hat{\sigma}_a+\sigma_{bn}}}{1-\sum_n w_{an}\dfrac{\sigma_{an}}{\sigma_{an}+\hat{\sigma}_a+\sigma_{bn}}}, \tag{2.30}$$

where $\hat{\sigma}_g$ is the total absorption cross section of the other resonant nuclides. The effective self-shielded cross sections are estimated iteratively.

2.3.2 Subgroup data generation

The RI_x is defined as the numerator of Eq. (2.24), and the RI divided by lethargy width is also called R_x. The RI can be written as Eq. (2.31) by using the subgroup weights and levels from Eq. (2.29).

$$R_x = \sum_n w_n\sigma_{xn}\frac{\sigma_{bn}}{\sigma_{an}+\sigma_{bn}} \approx \sum_n w_n\sigma_{xn}\frac{\sigma_b}{\sigma_{an}+\sigma_b}. \tag{2.31}$$

Since the denominator of Eq. (2.24) can be understood as a scalar flux (ϕ) for the coarse energy group, Eq. (2.24) can be rewritten as follows:

$$\sigma_x = \frac{R_x}{\phi}. \tag{2.32}$$

As described previously, the constituent compositions and the geometrical configurations are varied to obtain various background cross sections to complete the RI table. Index '*k*' for the variation cases can be added to Eq. (2.32).

$$\sigma_{x,k} = \frac{R_{x,k}}{\phi_k} \quad (k = 1, 2, \ldots, K). \tag{2.33}$$

The RI ($R_{x,k}$) can be estimated directly from the IRFFACTOR program for the variation cases. The subgroup levels and weights can be obtained from Eq. (2.31) by the least square fitting to minimize the difference between the original RI and the reconstructed RI using Eq. (2.31). Subgroup levels are arbitrary, and the corresponding subgroup weights are obtained by minimizing the following function *f*.

$$f(w_1,\ldots,w_K) = \sum_k \frac{1}{R_{x,k}^2}\left(R_{x,k} - \sum_n w_{xn}\sigma_{xn,k}\frac{\sigma_{bn,k}}{\sigma_{an,k}+\sigma_{bn,k}}\right)^2. \tag{2.34}$$

$$f(w_1,\ldots,w_K) = \sum_k \frac{1}{R_{x,k}^2}\left(R_{x,k} - \sum_n w_{xn}\sigma_{xn,k}\frac{\sigma_{b,k}}{\sigma_{an,k}+\sigma_{b,k}}\right)^2. \tag{2.35}$$

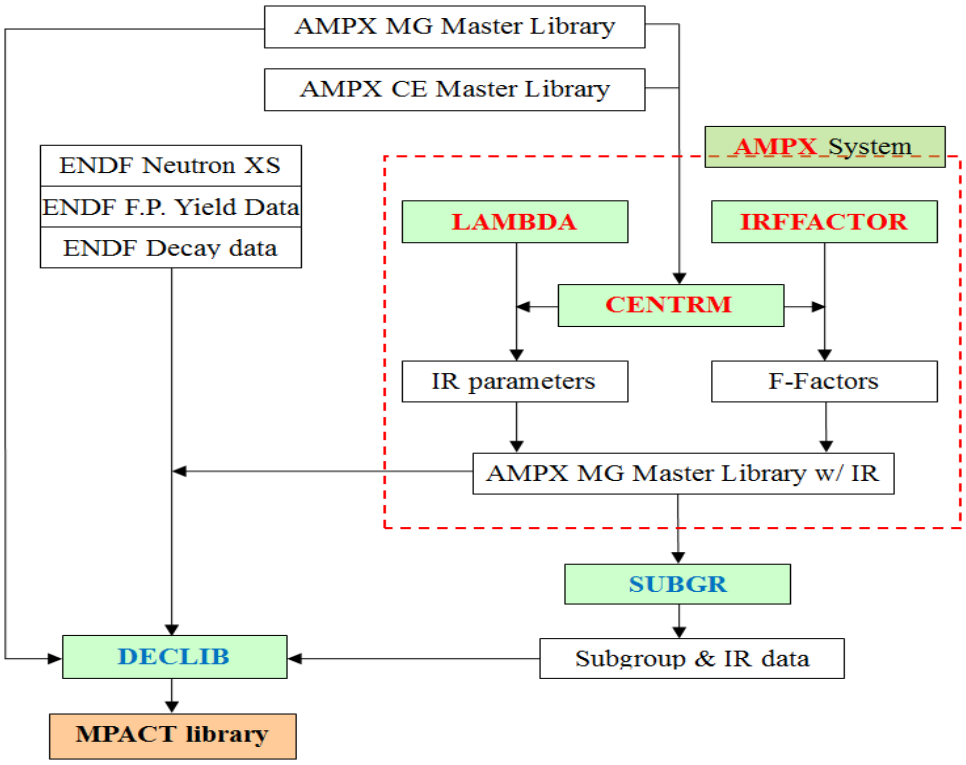

Figure 2.4 Resonance Data Generation Procedure.

Subgroup levels must be automatically adjusted to minimize the difference between the original RI and the reconstructed RI using the subgroup levels and weights. The RI table from the IRFFACTOR calculation includes the background cross sections as a function of the absorption cross section at each variation *k* to cover all the subgroup levels. Although the subgroup levels are varied at iterations, the corresponding background cross section ($\sigma_{bn,k}$) can be obtained through interpolation of the given table. SUBGR includes two options to generate the subgroup weights and levels by using Eq. (2.34), which uses the level dependent cross section, and Eq. (2.35), which uses the constant background cross section. Figure 2.4 provides a flow chart for generating the subgroup data.

When the resonance interference is neglected, errors in estimating the effective self-shielded cross section come mainly from the subgroup levels and weights themselves, as well as the scalar flux estimation. In the real application, the self-shielded scalar flux is estimated by the following equation.

$$\hat{\phi}_k = 1 - \sum_n w_{an} \frac{\sigma_{an,k}}{\sigma_{an,k} + \sigma_{bn,k}}, \tag{2.36}$$

where the subgroup weights and levels are given and the corresponding background cross sections ($\sigma_{bn,k}$) are obtained by the fixed source transport calculations of the

transport lattice code using Eq. (2.25). The difference between the scalar flux (ϕ_k) in Eq. (2.33) and the scalar flux ($\hat{\phi}_k$) in Eq. (2.36) causes a difference in the effective self-shielded cross section.

To remove this error, a new method [Joo09] has been proposed to generate the subgroup weights in which the subgroup weights are to be estimated to conserve the self-shielded cross sections as follows:

$$f(w_1,\ldots,w_K)=\sum_k \frac{1}{R_{x,k}^2}(\hat{R}_{x,k}-\sum_n w_{xn}\sigma_{xn,k}\frac{\sigma_{bn,k}}{\sigma_{an,k}+\sigma_{bn,k}})^2, \tag{2.37}$$

where

$$\hat{R}_{x,k}=\sigma_{x,k}\hat{\phi}_k=\sigma_{x,k}(1-\sum_n w_{an}\frac{\sigma_{an,k}}{\sigma_{an,k}+\sigma_{bn,k}}). \tag{2.38}$$

2.3.3 Subgroup method for nonuniform temperature distribution

In a heterogeneous system, the self-shielded resonance cross sections are estimated from the self-shielded scalar fluxes obtained by the following fixed source transport equation.

$$\hat{\Omega}\cdot\nabla\psi_{g,m}+\sum_i(\Sigma_{i,a,g}^m+\lambda_{i,g}\Sigma_{i,p})\psi_{g,m}(\hat{\Omega})=\sum_i\lambda_{i,g}\Sigma_{i,p}, \tag{2.39}$$

where subscript *m* denotes a problem case with different absorption cross section levels at energy group *g*. In Eq. (2.39), $\Sigma_{i,a,g}$ and $\Sigma_{i,p}$ denote macroscopic absorption and potential cross sections of nuclide *i*, respectively, and $\lambda_{i,g}$ IR parameter.

Equation (2.39) should be modified for the resonance transport calculations involving nonuniform temperature distribution in which the macroscopic absorption cross sections should include the temperature distribution, as follows:

$$\Sigma_{i,a,g}^m=N_i\sigma_{i,a,g}^m(T_{ave.})\frac{\sigma_{i,a,g}^m(T)}{\sigma_{i,a,g}^m(T_{ave.})}\approx N_i\sigma_{i,a,g}^m(T_{ave.})f_{i,a,g}(T), \tag{2.40}$$

where T and $T_{ave.}$ are local and volume-averaged temperatures, respectively. The function $f(T)$ was approximated by the following equation [Wem07].

$$f_{i,a,g}(T)=\frac{R_{i,a,g}(T,\sigma_p)}{R_{i,a,g}(T_{ave.},\sigma_p)}\cdot\frac{\sigma_p-R_{i,a,g}(T_{ave.},\sigma_p)}{\sigma_p-R_{i,a,g}(T,\sigma_p)}, \tag{2.41}$$

where

$$\sigma_p \approx \frac{\sum_{j=all} N_j \lambda_{j,g} \sigma_{j,p}}{N_i} , \tag{2.42}$$

N_i is the particle number density of nuclide i, and $R_{i,a,g}$ RI. Equation (2.45) can be rewritten without any approximation, as follows:

$$\sigma_{b,g}^m = \frac{\sum_{j=all} N_j \lambda_{j,g} \sigma_{j,p} + \Sigma_{e,g}^m}{N_i} . \tag{2.43}$$

Therefore, the explicit equation will be

$$f_{i,a,g}^m(T) = \frac{\sigma_{i,a,g}^m(T)}{\sigma_{i,a,g}^m(T_{ave})} = \frac{R_{i,a,g}(T,\sigma_{b,g}^m)}{R_{i,a,g}(T_{ave.},\sigma_{b,g}^m)} \cdot \frac{\sigma_{b,g}^m - R_{i,a,g}(T_{ave.},\sigma_{b,g}^m)}{\sigma_{b,g}^m - R_{i,a,g}(T,\sigma_{b,g}^m)} . \tag{2.44}$$

When performing a MPACT calculation with thermal-hydraulic feedback, $\Sigma_{e,g}^m$ can be obtained from the previous outer iteration.

Another better approximation is to obtain the correction factor from the previous step, as follows:

$$\Sigma_{i,a,g}^{m(\ell+1)} = N_i \sigma_{i,a,g}^m(T_{ave.}) \frac{\sigma_{i,a,g}^m(T)}{\sigma_{i,a,g}^m(T_{ave.})} \approx N_i \sigma_{i,a,g}^m(T_{ave.}) \frac{\sigma_{i,a,g}^{(\ell)}(T)}{\sigma_{i,a,g}^{(\ell)}(T_{ave.})} . \tag{2.45}$$

2.4 TRANSPORT CROSS SECTIONS FOR ^{1}H

The MOC eigenvalue calculation with high order (≥P_2) scattering requires 2 times more computing time compared to the P_0 calculation. Typically, most of transport lattice codes are using an out-scattering based transport corrected P_0 (TCP_0) scattering matrix in which the diagonal terms of the P_0 scattering matrix are subtracted by total P_1 scattering cross sections. The P_1 corrected P_0 scattering matrix for ^{1}H may include negative value in the diagonal components. This causes negative flux, resulting in convergence error. Another issue of out-scattering–based transport correction shows significant global power tilt for whole core problems, including reflectors. Therefore, a proper transport correction method is needed to have reasonable neutron leakage, as high order scattering is considered and to guarantee no negative flux.

The Neutron Leakage Conservation ($NLCP_0$) method [Her13] has been used to generate transport cross sections for ^{1}H. The goal of $NLCP_0$ is to obtain diffusion coefficients to have the same neutron leakage as that obtained in the high order scattering transport calculation, as follows:

$$\hat{\Omega}\cdot\nabla\varphi_g(\hat{\Omega}) = -D_g\nabla^2\phi_g\,. \tag{2.46}$$

With a one-dimensional slab model, neutron leakages at the specified surfaces can be obtained from the high order scattering transport calculation.

$$Leakage = J_{right} - J_{left}\,. \tag{2.47}$$

Diffusion coefficients can be determined to have same leakage in the diffusion calculation by using the following derivation.

$$-D\nabla^2\phi + \Sigma_a\phi = \frac{1}{k_{eff}}\nu\Sigma_f\phi\,. \tag{2.48}$$

$$\nabla^2\phi + B^2\phi = 0 \;\rightarrow\; \frac{\partial^2}{\partial x^2}\phi(x) + B^2\phi(x) = 0\,. \tag{2.49}$$

$$\phi(x) = \cos(Bx)\,. \tag{2.50}$$

$$J_{right} - J_{left} = \int_0^W dx(-D\frac{\partial^2}{\partial x^2}\phi(x)) = \int_0^W dxDB^2\phi(x) = DB^2\int_0^W dx\phi(x) = DB^2\hat{\phi}\,. \tag{2.51}$$

$$D = \frac{J_{right} - J_{left}}{B^2\hat{\phi}}\,. \tag{2.52}$$

$$B^2_{geom} = \left(\frac{\pi}{W}\right)^2\,. \tag{2.53}$$

When performing the MG transport calculation with high order scattering, he group-wise bucklings must be checked to ensure that they are constant, independent of the energy group. This work can be completed by drawing a normalized neutron spectrum shape for each group.

$$B^2_{geom} = B^2 = B^2_g\,. \tag{2.54}$$

Multigroup diffusion coefficients and transport cross sections can be obtained as follows:

$$D_g = \frac{J_{g,right} - J_{g,left}}{B^2\hat{\phi}_g}\,. \tag{2.55}$$

$$\Sigma_{tr,g} = \frac{1}{3D_g}\,. \tag{2.56}$$

This computational model is from Herman et al. [Her13], as follows:

- slab 100 cm w/ vacuum boundary, 0.005 cm mesh size,
- all ^{1}H with 4.780E+23 atom/cm^3,

- 9 temperatures: 293.6, 350, 400, 450, 500, 550, 600, 650, 800 K, and
- source: ^{235}U fission spectrum with buckled cosine spatial distribution.

A new SCALE procedure—h1TransportXS—is based on one-dimensional slab discrete ordinate transport calculation and has been developed to generate transport correction factors by using the NLC method. Figure 2.5 provides the 51-group transport correction factors for ^{1}H with various temperatures.

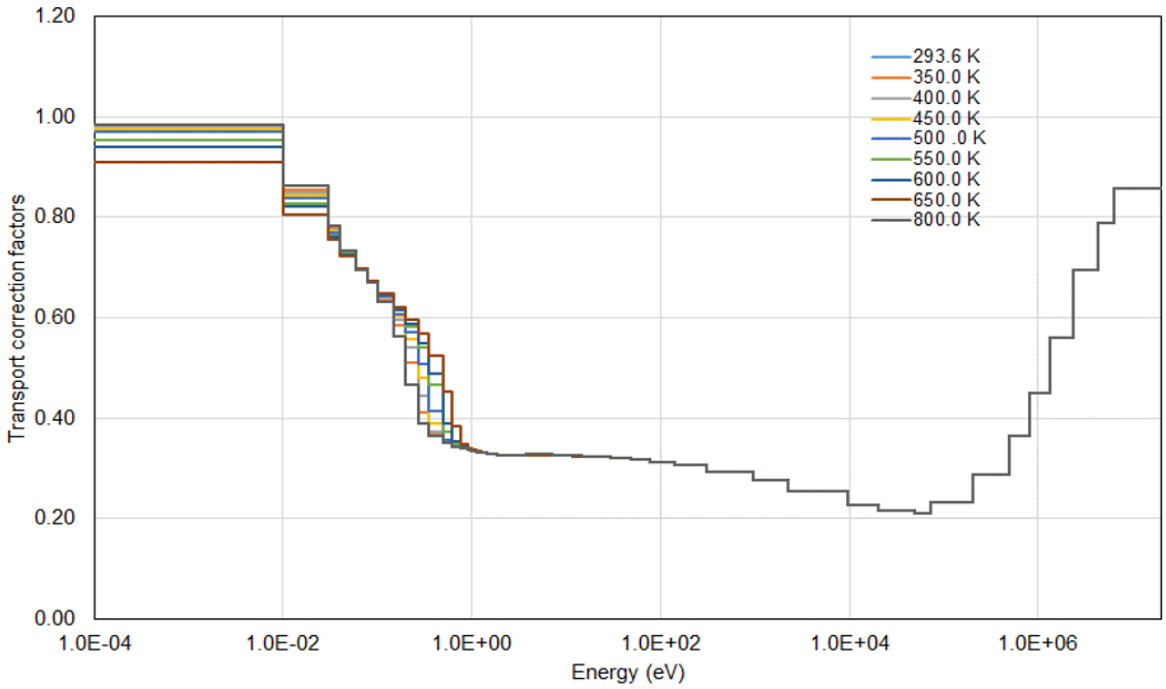

Figure 2.5. 51-Group Transport Correction Factors for ^{1}H.

2.5 SPH METHOD FOR THE ^{238}U SUBGROUP DATA

Energy group collapsing from fine to coarse groups introduces angle-dependent total cross sections and high order flux moment weighted scattering matrices. Since the angular fluxes and high order flux moments are problem dependent, it is not possible to generate the coarse energy group resonance data and scattering matrices considering angle dependency of nuclear data. In addition, self-shielded cross section tables are generated by considering the resonance interference effect between resonance nuclides such as ^{238}U and ^{235}U in the CENTRM PW slowing down calculation. This method may provide better agreement for the specific cases in MG resonance self-shielded cross sections or reaction rates between the reference and MPACT solutions. However, resonance interferences are doubly considered due to the Bondarenko iteration of subgroup method for resonance interference, and this procedure would introduce significant ^{235}U enrichment bias, resulting in radial power tilt at the whole core calculation.

A new SPH method has been developed to address the issues described above by conserving reaction rates between high order reference solutions and the low order MPACT calculations. The procedure in Figure 2.6 starts with the KENO models, including the same variation cases shown in Table 2.1 as the heterogeneous IRFFACTOR cases. Then the MG self-shielded cross sections are tallied, and the corresponding background cross sections are estimated by the ESSM calculations to complete the self-shielded cross section tables. The subgroup data are generated by SUBGR and incorporated into the MPACT MG library, and then the MPACT calculations are performed for the same variation cases to obtain the group-wise SPH factors defined in Eq. (2.57).

$$f_{x,g,i}^{n+1} = \frac{\sigma_{x,g,i}^{n}\phi_{x,g,i}^{n}}{\sigma_{x,g,i}^{keno}\phi_{x,g,i}^{keno}}, \tag{2.57}$$

$$\sigma_{x,g,i}^{n+1} = f_{x,g,i}^{n+1}\sigma_{x,g,i}^{n}. \tag{2.58}$$

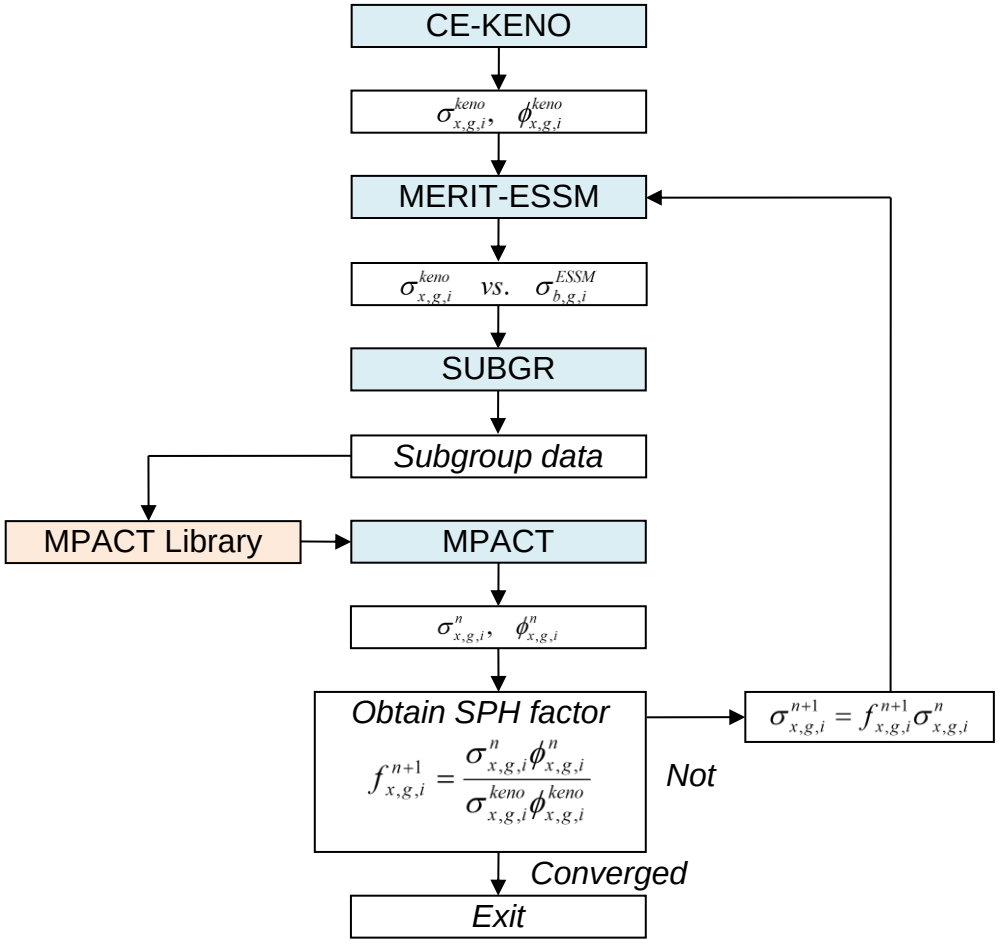

Figure 2.6. SPH Method to Generate the ^{238}U Subgroup Data.

Newly adjusted self-shielded cross section tables are generated by using Eq. (2.58) and new corresponding background cross sections, and then new subgroup data are produced accordingly. The SPH factors can be selectively applied to the specified energy groups indicating significant reaction rate differences. Figure 2.7 compares reaction rate differences for ^{238}U with and without SPH factors. The differences are obtained from a comparison between the MPACT and CE-KENO reaction rates. The result indicates significant improvements in the largest resonance and high-energy resonances. This SPH method is simple and does not require any modification of the cross section library format. And this method effectively resolves the issues of angle-dependent total cross sections, resonance interference, and P_0 flux moment weighted scattering matrices.

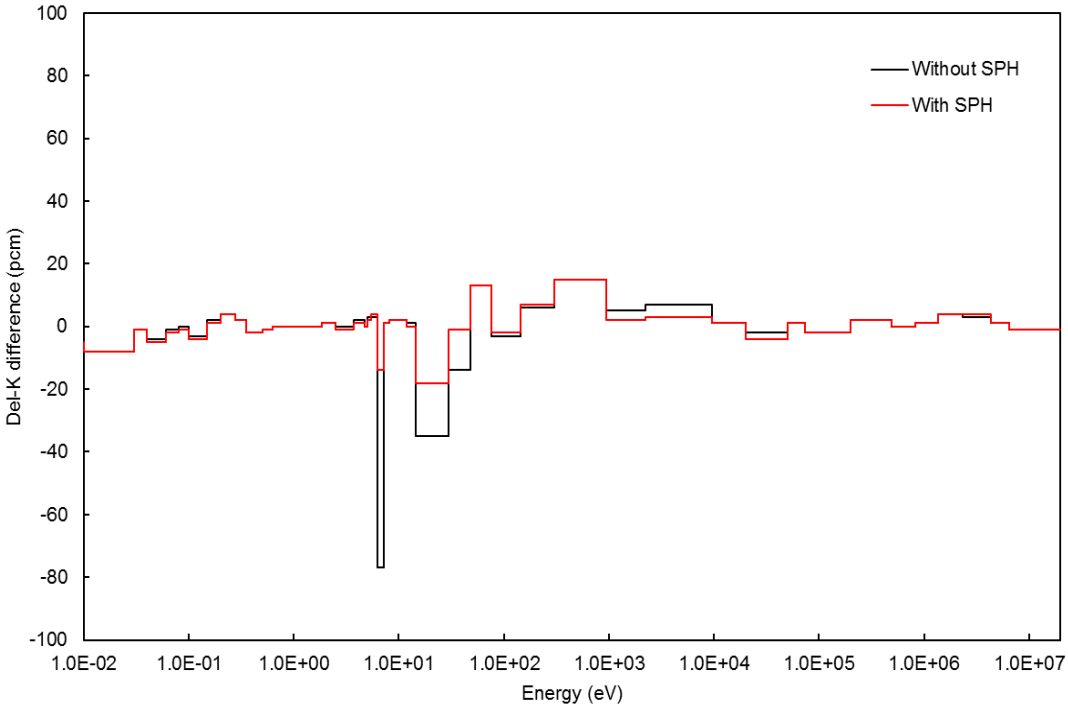

Figure 2.7. ^{238}U 51-Group Absorption Reaction Rate Differences with/without SPH Factors.

3 THE IMPACT 51-GROUP LIBRARY GENERATION

A new ENDF/B-VII.1 v4.3m1 MPACT 51-group library was developed by the AMPX/SCALE and CASL XSTools code packages. The 51-group structure was developed to be a subset of the SCALE-6.2 ENDF/B-VII.1 252-group referring to the HELIOS-1.9 47-group structures, with evenly distributed group widths to exclude a stability issue due to negative cross sections that occur when performing transport corrected P_0 calculations. Table 3.1 provides the 51-group structure; groups 10–31 include resonance and subgroup data.

Table 3.1. The 51-Group Structure

Group	Upper bound	Group	Upper bound	Group	Upper bound
1	2.000000E+07	18	4.830000E+01	35	1.080000E+00
2	6.434000E+06	19	3.000000E+01	36	1.010000E+00
3	4.304000E+06	20	1.440000E+01	37	9.750000E-01
4	2.354000E+06	21	1.190000E+01	38	9.250000E-01
5	1.356000E+06	22	8.100000E+00	39	7.500000E-01
6	8.200000E+05	23	7.150000E+00	40	6.250000E-01
7	4.920000E+05	24	6.250000E+00	41	5.000000E-01
8	2.000000E+05	25	5.400000E+00	42	3.500000E-01
9	7.300000E+04	26	5.000000E+00	43	2.750000E-01
10	5.000000E+04	27	4.700000E+00	44	2.000000E-01
11	2.000000E+04	28	3.730000E+00	45	1.500000E-01
12	9.500000E+03	29	2.470000E+00	46	1.000000E-01
13	2.250000E+03	30	1.860000E+00	47	8.000000E-02
14	9.500000E+02	31	1.450000E+00	48	6.000000E-02
15	3.050000E+02	32	1.250000E+00	49	4.000000E-02
16	1.430000E+02	33	1.175000E+00	50	3.000000E-02
17	7.600000E+01	34	1.130000E+00	51	1.000000E-02

3.1 AMPX 51-GROUP LIBRARY

The ENDF/B-VII.1 AMPX 51-group library was generated by using the AMPX EXSITE utility to generate the AMPX input files for all nuclides by expanding a template. Figure 2.1 provides the AMPX procedure to generate the AMPX MG library, where the left side of the flow chart is for the conventional procedure, and the right side is for the new procedure that improves the Bondarenko resonance data. After completing the AMPX calculations for all nuclides, individual MG data files can be merged into an initial AMPX MG library using the AMPX AJAX module.

The IR parameters are generated for all nuclides by using the AMPX LAMBDA module using a procedure introduced in Section 2.2.1 in which the IR parameters are estimated only for the specified energy groups and unity is assigned to other energy groups. In addition, homogeneous Bondarenko F-factors (resonance self-shielded cross sections) are generated for nuclides with ≥ 40 (Zr) atomic number, substituting the original F-factors based on the NR approximation.

Only selected resonance nuclides include heterogeneous F-factors; they have been determined to be important resonance nuclides because they can significantly impact

the neutronics result. The 23 nuclides listed below were selected to have heterogeneous F-factors. The subgroup data for these nuclides were generated by conserving cross sections.

- ^{107}Ag, ^{109}Ag, ^{113}Cd, ^{113}In, ^{115}In, ^{133}Cs, ^{155}Eu, ^{155}Gd, ^{156}Gd, ^{157}Gd, ^{158}Gd, ^{167}Er, ^{232}Th, ^{233}U, ^{235}U, ^{236}U, ^{238}U, ^{238}Pu, ^{239}Pu, ^{240}Pu, ^{241}Pu, ^{242}Pu, and ^{241}Am

Since the Bondarenko approach is not typically capable of addressing resonance interference effects explicitly, heterogeneous F-factors can be generated in two different ways, with or without consideration of explicit resonance interference. The term *single* indicates without resonance interference, and *Multiple* indicates with resonance interference. The single absorber model has only been applied to 4 nuclides, including ^{113}Cd, ^{113}In, ^{115}In and ^{238}U.

The heterogeneous IRFFACTOR results in two F-factor tables, the first of which can be incorporated by AMPX AJAX, and the second (subgrpdata) is for SUBGR to generate subgroup data. The first table (the AMPX MG master library) can also be used in subgroup data generation. However, to generate subgroup data to conserve cross sections, subgroup-level–dependent background cross sections should be added to the F-factor tables (self-shielded cross section table). The AMPX MG library does not include the subgroup-level–dependent background cross sections, but the subgrpdata file includes them.

3.2 MPACT 51-GROUP LIBRARY

The Bondarenko F-factors in the AMPX MG library should be converted into RI tables to be used in the subgroup data generation. Then the subgroup data are generated by using SUBGR. Subgroup data including weights and levels have been generated for 49 important resonance nuclides, as shown in Table 3.2 for all energy groups.

Table 3.2 List of Nuclides, Including Subgroup Data

No.	Nuclide	No.	Nuclide	No.	Nuclide	No.	Nuclide	No.	Nuclide
1	^{91}Zr	11	^{131}Xe	21	^{157}Gd	31	^{177}Hf	41	^{235}U
2	^{96}Zr	12	^{133}Cs	22	^{158}Gd	32	^{178}Hf	42	^{236}U
3	^{95}Mo	13	^{152}Sm	23	^{160}Dy	33	^{179}Hf	43	^{238}U
4	^{99}Tc	14	^{151}Eu	24	^{161}Dy	34	^{180}Hf	44	^{238}Pu
5	^{103}Rh	15	^{152}Eu	25	^{162}Dy	35	^{182}W	45	^{239}Pu
6	^{108}Pd	16	^{153}Eu	26	^{163}Dy	36	^{183}W	46	^{240}Pu
7	^{107}Ag	17	^{154}Eu	27	^{164}Dy	37	^{184}W	47	^{241}Pu
8	^{109}Ag	18	^{155}Eu	28	^{166}Er	38	^{186}W	48	^{242}Pu
9	^{113}In	19	^{155}Gd	29	^{167}Er	39	^{232}Th	49	^{241}Am
10	^{115}In	20	^{156}Gd	30	^{176}Hf	40	^{233}U		

The following data files are required for DECLIB to generate the MPACT MG library.

- AMPX MG library,

- ENDF/B files: neutron data, decay constants, fission product yields,
- subgroup data and RI table (49 nuclides, groups 10-31 in 51-g),
- transport correction factors (^{1}H),
- predetermined background cross sections (105 nuclides),
- transient data (21 nuclides), and
- subgroup data with epithermal upscattering (^{238}U).

Two sets of ^{238}U subgroup data with and without considering epithermal upscattering have been generated by using the SPH method introduced in Section 2.5, for which the CE KENO calculations were performed without and with the Doppler broadening rejection correction (DBRC) [Bec10] option. The MPACT MG library includes ^{238}U resonance and subgroup data with and without considering epithermal upscattering, one of which will be used according to a MPACT user option.

Figure 3.1 provides a flow diagram of DECLIB to generate the MPACT MG library. The required data for the steady-state transport calculation are the transport cross section, fission cross section, the average number of neutrons released from a fission reaction, and the fission spectrum for each nuclide. Since the absorption and fission cross sections are modified through the resonance treatment and are needed for the depletion calculation, those cross sections should be included. The (n,2n) and (n,3n) cross sections are required for the depletion calculation. High order (P_1– P_3) scattering matrices are also included. Therefore, the multigroup data required in the library are as follows:

a. transport cross section (σ_{tr})
b. absorption cross section ($\sigma_{a}= \sigma_{c}+\sigma_{f}$)
c. fission cross section (σ_{f})
d. neutrons released from a fission (ν)
e. scattering cross sections ($\sigma_{s0\sim3}$)
f. (n,2n) cross section ($\sigma_{n,2n}$)
g. (n,3n) cross section ($\sigma_{n,3n}$)
h. $P_{0\sim3}$ scattering matrix ($\sigma_{sngg'}$)
i. fission spectrum (χ_{g})

Since the AMPX MG master library includes cross section data for various reactions, cross sections must be merged to generate the underlined data shown above.

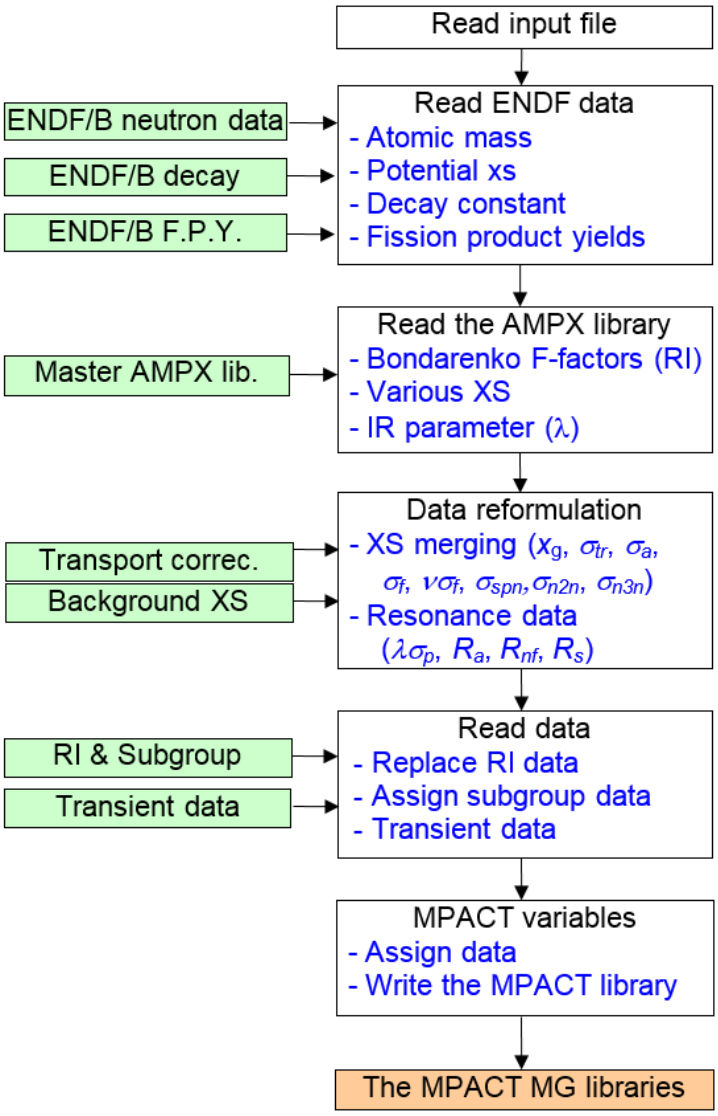

Figure 3.1. DECLIB Calculation Flow.

4 VERIFICATION AND VALIDATION

4.1 VERA CORE PHYSICS BENCHMARK PROGRESSION PROBLEMS

4.1.1 Characteristics of Benchmark Problems

The VERA core physics benchmark progression problems were created to provide a method for developing and demonstrating increasing capabilities for reactor physics methods and software [God14]. The progression problems range from a simple 2D pin cell to the full cycle depletion and refueling of a 3D reactor core configuration with control rods and burnable poisons consistent with actual nuclear power plant designs. Most of the data are based on fuel and plant data from the initial core loading of Watts Bar Nuclear 1, a Westinghouse-designed 17 × 17 pressurized water reactor (PWR) of the common vintage built in the United States during the 1980s and 1990s.

Table 4.1. Details of the VERA Progression Problems

Problem		Description	^{235}U w/o	Temperature (K)			Moderator	
				Mod.	Clad	Fuel	g/cm^3	PPM
1	1A	PWR pin	3.1	565	565	565	0.743	1300
	1B	PWR pin	3.1	600	600	600	0.661	1300
	1C	PWR pin	3.1	600	600	900	0.661	1300
	1D	PWR pin	3.1	600	600	1200	0.661	1300
	1E	PWR pin + integral fuel burnable absorber (IFBA)	3.1	600	600	600	0.743	1300
2	2A	PWR FA, no BP	3.1	565	565	565	0.743	1300
	2B	PWR FA, no BP	3.1	600	600	600	0.661	1300
	2C	PWR FA, no BP	3.1	600	600	900	0.661	1300
	2D	PWR FA, no BP	3.1	600	600	1200	0.661	1300
	2E	PWR FA + 12 Pyrex	3.1	600	600	600	0.743	1300
	2F	PWR FA + 24 Pyrex	3.1	600	600	600	0.743	1300
	2G	PWR FA + 24 AIC CR	3.1	600	600	600	0.743	1300
	2H	PWR FA + 24 B_4C CR	3.1	600	600	600	0.743	1300
	2I	PWR FA + Instrument Thimble	3.1	600	600	600	0.743	1300
	2J	PWR FA + Instrument Thimble + 24 Pyrex	3.1	600	600	600	0.743	1300
	2K	PWR FA + Zoned enrichment + 24 Pyrex	3.1/3.6	600	600	600	0.743	1300
	2L	PWR FA + 80 IFBA	3.1	600	600	600	0.743	1300
	2M	PWR FA + 128 IFBA	3.1	600	600	600	0.743	1300
	2N	PWR FA + 104 IFBA + 20 WABA	3.1	600	600	600	0.743	1300
	2O	PWR FA + 12 Gadolinia	1.8/3.1	600	600	600	0.743	1300
	2P	PWR FA + 24 Gadolinia	1.8/3.1	600	600	600	0.743	1300
	2Q	PWR FA + Zircaloy Spacer grid	3.1	565	565	565	0.743	1300
5	5A-2D	PWR 2D core	2.1/2.6/3.1	565	565	565	0.743	1285
	5B-2D	PWR 2D core B_4C Control rod	2.1/2.6/3.1	565	565	565	0.743	1285
	5C-2D	PWR 2D core AIC Control rod	2.1/2.6/3.1	565	565	565	0.743	1285
	5A-3D	PWR 3D core	2.1/2.6/3.1	565	565	565	0.743	1285

The single-physics 2D benchmark problems were selected for the evaluating the neutron cross section library for the VERA neutronics simulator MPACT. Table 4.1 lists the selected VERA progression problems used for this benchmarking. Figure 4.1 provides layouts of the pins and assemblies. Godfrey [God14] provides detailed

specifications of geometry and composition. The reference solutions were obtained using KENO with ENDF/B-VII.1 with and without the DBRC option.

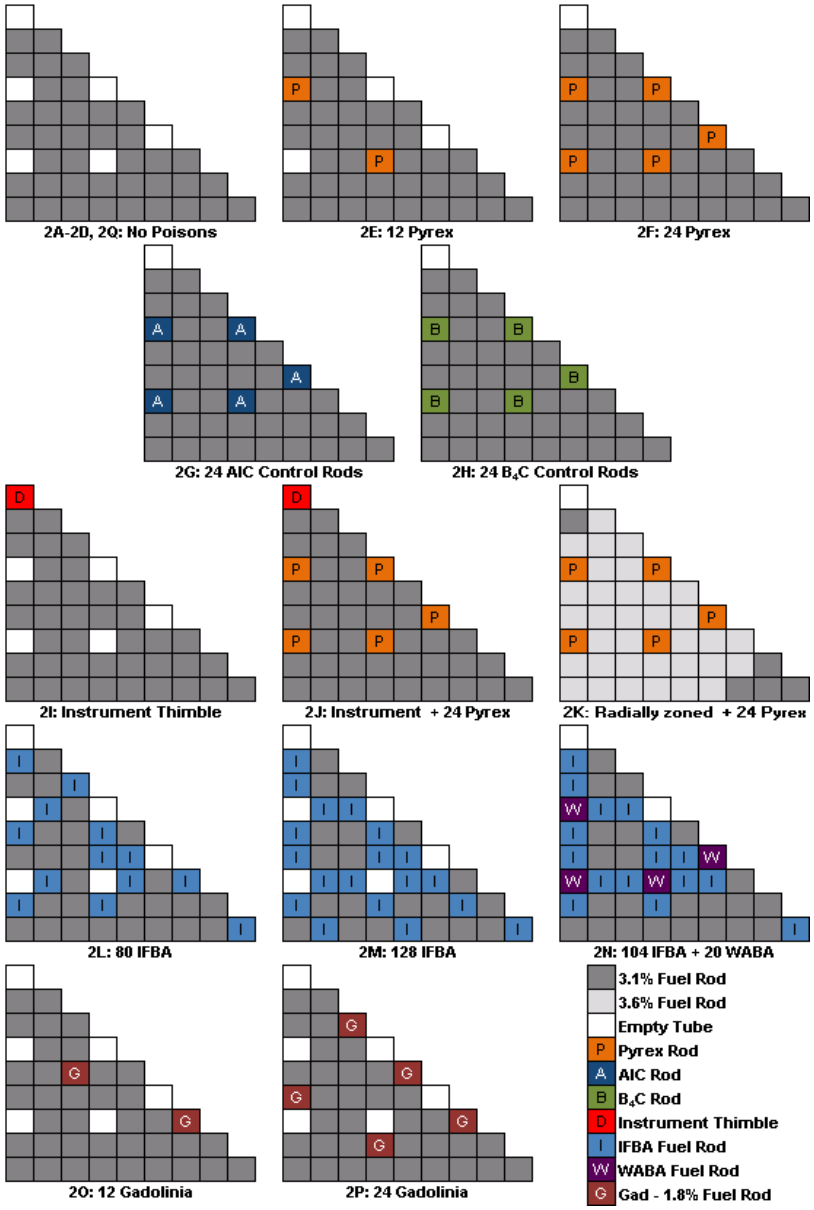

Figure 4.1. Problem 2 lattice Layouts (Octant Symmetry).

4.1.2 Benchmark Results

Benchmark calculations were performed by using the ENDF/B-VII.1 v4.3m1 MPACT 51-group library with and without epithermal upscattering. Tables 4.1 and 4.2 provide benchmark results using the ENDF/B-7.1 MPACT 51-g library with and without considering epithermal upscattering. The benchmark results are summarized as follows:

- All of the MPACT P_2 results satisfy the accuracy goals for prediction of multiplication factors (< 200 pcm $\Delta\rho$ or Δk) and pin power distributions.
- ^{238}U epithermal upscattering resonance data (DBRC option in Monte Carlo) have been generated correctly.
- No temperature reactivity bias is not observed.
- Since the transport cross sections of ^{1}H have been generated to conserve neutron leakage for the whole core problems, there are some reactivity differences for single pin and assembly problems when performing transport-corrected P_0 (TCP_0) calculations.
- Cases 2G and 2H are control rod insertion cases which show significant k_{eff} differences when performing TCP_0 calculations. The TCP_0 calculation is not able to correctly simulate highly anisotropic neutron angular fluxes in and around control rods in single-lattice rodded problems, but these errors dissipate in full-core calculations. Similar issues are observed for the burnable poison–bearing cases, even though k_{eff} differences are not significant.
- Prediction of the power distribution is good for all cases, regardless of the number of energy groups.

Table 4.2. Results with the ENDF/B-7.1 MPACT 51-g Library

Case	Epithermal upscattering							No epithermal upscattering						
	KENO	MPACT P_2[b]			MPACT TCP0[c]			KENO	MPACT P_2[b]			MPACT TCP_0[c]		
	k_{eff}	Δk pcm	Pin power %		Δk pcm	Pin power %		k_{eff}	Δk pcm	Pin power %		Δk pcm	Pin power %	
			SD	Max.		SD	Max.			SD	Max.		SD	Max.
1A	1.18569	-27	-	-	-45	-	-	1.18700	-24			-45		
1B	1.18065	-14	-	-	-51	-	-	1.18214	-12			-52		
1C	1.16895	-5	-	-	-49	-	-	1.17144	-22			-68		
1D	1.15885	-3	-	-	-53	-	-	1.16258	-23			-76		
1E	0.77082	-168	-	-	-141	-	-	0.77127	-204			-177		
2A	1.18081	-76	0.12	-0.33	-48	0.12	-0.30	1.18187	-85	0.12	0.25	-59	0.12	0.26
2B	1.18190	-38	0.11	0.21	-30	0.11	-0.23	1.18323	-37	0.13	0.31	-32	0.14	0.32
2C	1.17125	-31	0.13	0.29	-29	0.12	0.30	1.17362	-34	0.12	-0.23	-34	0.13	0.29
2D	1.16189	-45	0.11	0.34	-48	0.11	0.36	1.16556	-34	0.13	0.37	-39	0.13	0.32
2E	1.06829	-71	0.14	-0.25	-120	0.10	-0.23	1.06953	-58	0.15	-0.44	-109	0.13	-0.40
2F	0.97462	-96	0.18	0.43	-175	0.17	-0.46	0.97569	-92	0.16	0.41	-173	0.15	0.43
2G	0.84674	-140	0.22	-0.45	-375	0.25	-0.58	0.84766	-135	0.23	0.47	-372	0.26	-0.66
2H	0.78705	-145	0.23	0.58	-494	0.27	0.70	0.78793	-136	0.24	-0.67	-486	0.30	-0.90
2I	1.17865	-65	0.12	0.29	-40	0.13	0.29	1.17962	-90	0.14	0.33	-67	0.14	0.30
2J	0.97378	-104	0.14	-0.33	-183	0.14	0.33	0.97496	-89	0.17	-0.44	-170	0.16	-0.42
2K	1.01864	-115	0.17	0.34	-189	0.17	-0.38	1.01977	-108	0.14	0.36	-183	0.14	0.31
2L	1.01760	-153	0.15	-0.37	-132	0.15	-0.40	1.01868	-148	0.13	0.37	-128	0.13	0.34
2M	0.93778	-152	0.12	-0.25	-123	0.14	-0.33	0.93855	-168	0.15	0.32	-141	0.16	-0.41
2N	0.86840	-129	0.19	0.44	-166	0.13	-0.30	0.86944	-113	0.22	0.64	-151	0.16	0.51
2O	1.04613	-91	0.16	-0.39	-183	0.16	-0.42	1.04717	-93	0.18	0.43	-188	0.17	0.44
2P	0.92566	-117	0.23	-0.51	-284	0.21	0.47	0.92670	-104	0.21	-0.46	-273	0.19	-0.46

[a] SD: standard deviation
[b] P2: P_2 scattering
[c] TCP0: transport correct P_0 scattering

Table 4.3 and Figure 4.2 provide benchmark results for the VERA progression 5A-2D, 5B-2D and 5C-2D quarter core problems by using the v4.3m1 MPACT and 51-group library. The reference solutions were obtained by using CE-KENO with the ENDF/B-7.1 nuclear data with and without considering epithermal upscattering. The benchmark results are very consistent with the reference CE-KENO result for both multiplication factors and pin power distributions.

Table 4.3. Results for 2D Core Problems with the ENDF/B-7.1 Library.

Epithermal upscattering	Case	KENO* k_{eff}	MPACT P_2			MPACT TCP_0		
			Δk_{eff} (pcm)	pin power diff. (%)		Δk_{eff} (pcm)	pin power diff. (%)	
				Max.	RMS		Max.	RMS
No	5A-2D	1.00370	-86	1.78	0.76	-97	1.10	0.45
	5B-2D	0.99113	-89	2.00	0.94	-101	1.23	0.47
	5C-2D	0.98979	-71	2.29	0.98	-106	1.21	0.47
Yes	5A-2D	1.00273	-83	-	-	-91	-	-
	5B-2D	0.99013	-89	-	-	-100	-	-
	5C-2D	0.98893	-81	-	-	-91	-	-

*S.D. < 0.00005

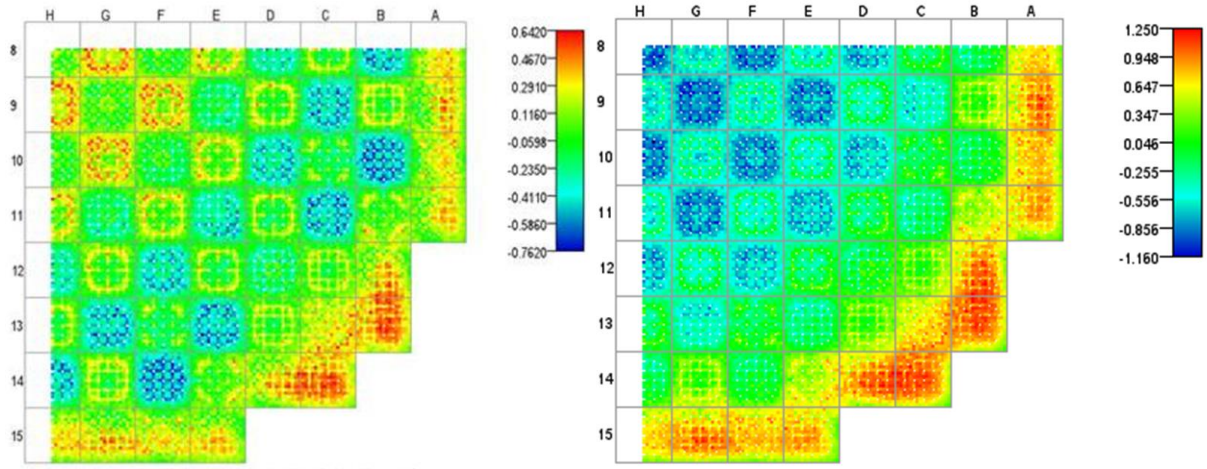

(a) Epithermal upscattering (b) No epithermal upscattering

Figure 4.2. Pin Power Comparisons for Problem 5A-2D.

4.2 EXTENDED VERA BENCHMARK PROGRESSION PROBLEMS

4.2.1 Characteristics of Problems

Since the VERA core physics benchmark progression problems do not include various ^{235}U enrichment and burnup compositions, additional benchmark problems have been developed to determine the sensitivities of the libraries to ^{235}U enrichment, burnup, and the number of radial fuel rings. These benchmark problems are based on VERA progression problems 1B and 1C. Table 4.4 provides a list of new extended VERA benchmark problems. Cases 1C-10-1h through 1C-60-1h include only heavy nuclides and exclude fission product isotopes.

Table 4.4. Extended VERA Benchmark Problems

Case	Description	^{235}U w/o	Burnup (MWD/kgU)	Temperature (K)			Moderator	
				Mod.	Clad	Fuel	g/cm^3	PPM
1B-21	PWR pin ^{235}U 2.1 w/o	2.1	0	600	600	600	0.661	1300
1B-26	PWR pin ^{235}U 2.6 w/o	2.6	0	600	600	600	0.661	1300
1B-31	PWR pin ^{235}U 3.1 w/o	3.1	0	600	600	600	0.661	1300
1B-36	PWR pin ^{235}U 3.6 w/o	3.6	0	600	600	600	0.661	1300
1B-41	PWR pin ^{235}U 4.1 w/o	4.1	0	600	600	600	0.661	1300
1B-46	PWR pin ^{235}U 4.6 w/o	4.6	0	600	600	600	0.661	1300
1C-00-3a	PWR pin 3-ring, full isotopes	3.1	0	600	600	900	0.661	1300
1C-10-3a	PWR pin 3-ring, full isotopes	3.1	10	600	600	900	0.661	1300
1C-20-3a	PWR pin 3-ring, full isotopes	3.1	20	600	600	900	0.661	1300
1C-40-3a	PWR pin 3-ring, full isotopes	3.1	40	600	600	900	0.661	1300
1C-60-3a	PWR pin 3-ring, full isotopes	3.1	60	600	600	900	0.661	1300
1C-10-1h	PWR pin 1-ring, heavy isotopes	3.1	10	600	600	900	0.661	1300
1C-20-1h	PWR pin 1-ring, heavy isotopes	3.1	20	600	600	900	0.661	1300
1C-40-1h	PWR pin 1-ring, heavy isotopes	3.1	40	600	600	900	0.661	1300
1C-60-1h	PWR pin 1-ring, heavy isotopes	3.1	60	600	600	900	0.661	1300

4.2.2 Benchmark Results

Benchmark calculations have been performed using the ENDF/B-VII.1 MPACT 51-group library with and without considering epithermal upscattering. The benchmark results can be summarized as follows:

- As shown in the benchmark results in Section 4.1, there is a difference of about 40 pcm between P_2 and TCP_0 for fresh single pin problems. However, very large k_{eff} differences are observed for high burnup fuel cases such as 1C-40_1h and 1C-60_1h.
- There is no ^{235}U enrichment reactivity bias.

Table 4.5. Benchmark Result with the ENDF/B-7.1 MPACT 51-g Library

Case	Epithermal Upscattering			No epithermal Upscattering		
	KENO	KENO-MPACT (pcm)		KENO	KENO-MPACT (pcm)	
	k_{inf}	P_2	TCP_0	k_{inf}	P_2	TCP_0
1C-21	1.06871	-21	-50	1.07002	-30	-62
1C-26	1.13385	-17	-51	1.13548	0	-36
1C-31	1.18048	-30	-68	1.18211	-15	-55
1C-36	1.21951	-19	-60	1.22096	-23	-66
1C-41	1.25125	2	-42	1.25244	-28	-74
1C-46	1.27712	-25	-71	1.27871	-15	-63
1C-00-3a	1.24435	54	-3	1.24720	64	5
1C-10-3a	1.08484	-113	-174	1.08738	-94	-158
1C-20-3a	1.00059	-35	-129	1.00297	-11	-107
1C-40-3a	0.88112	38	-80	0.88297	41	-80
1C-60-3a	0.80711	16	-106	0.80869	12	-112
1C-10-1h	1.17128	-64	-133	1.17394	-57	-128
1C-20-1h	1.11417	62	-44	1.11647	46	-63
1C-40-1h	1.03382	161	25	1.03614	166	27
1C-60-1h	0.98625	194	51	0.98849	204	58

4.3 VERA DEPLETION BENCHMARK PROBLEMS

4.3.1 Characteristics of Problems

The VERA depletion benchmark problems [Kim16a] have been developed based on the VERA progression problems [God14]. Kim [Kim16a] provides the detailed geometrical and material data for the benchmark problems from VERA progression problems #1 and #2. The depletion benchmark suite includes 8 single pin problems and 16 fuel assembly problems with various fuel temperatures, ^{235}U enrichments, control rods, and burnable poisons, as shown in Table 4.6. The pin configurations of fuel rods, guide/instrument tubes, and burnable poisons are shown in Figure 4.6.

Table 4.6. Single Pin and Assembly Depletion Benchmark Problems

Case	Description	Temperature (K)			Moderator Density (g/cc)	^{235}U w/o	Power density (w/gU)
		Moderator	Clad	Fuel			
1A	Pin 3.1w/o T_F=565K	565	565	565	0.743	3.1	40.0
1B	Pin 3.1w/o T_F=600K	600	600	600	0.700	3.1	40.0
1C	Pin 3.1w/o T_F=900K	600	600	900	0.700	3.1	40.0
1D	Pin 3.1w/o T_F=1200K	600	600	1,200	0.700	3.1	40.0
1E	Pin IFBA 3.1w/o T_F=600K	600	600	900	0.700	3.1	40.0
1F	Pin 2.1w/o T_F=900K	600	600	900	0.700	2.1	40.0
1G	Pin 3.6w/o T_F=900K	600	600	900	0.700	3.6	40.0
1H	Pin 4.6w/o T_F=900K	600	600	900	0.700	4.6	40.0
2A	FA No Poisons T_F=565K	565	565	565	0.743	3.1	40.0
2B	FA No Poisons T_F=600K	600	600	600	0.700	3.1	40.0
2C	FA No Poisons T_F=900K	600	600	900	0.700	3.1	40.0
2D	FA No Poisons T_F=1200K	600	600	1,200	0.700	3.1	40.0
2E	FA 12 Pyrex	600	600	900	0.700	3.1	40.0
2F	FA 24 Pyrex	600	600	900	0.700	3.1	40.0
2G	FA 24 AIC	600	600	900	0.700	3.1	40.0
2H	FA 24 B4C	600	600	900	0.700	3.1	40.0
2I	FA Instrument Thimble	600	600	900	0.700	3.1	40.0
2J	FA Instrument + 24 Pyrex	600	600	900	0.700	3.1	40.0
2K	FA Zoned + 24 Pyrex	600	600	900	0.700	3.1/3.6	40.0
2L	FA 80 IFBA	600	600	900	0.700	3.1	40.0
2M	FA 128 IFBA	600	600	900	0.700	3.1	40.0
2N	FA 104 IFBA + 20 WABA	600	600	900	0.700	3.1	40.0
2O	FA 12 Gadolinia	600	600	900	0.700	3.1/1.8	40.0
2P	FA 24 Gadolinia	600	600	900	0.700	3.1/1.8	40.0

The computational results of the depletion calculations would depend on user options and libraries. Therefore, to minimize differences due to the user and library options, the following options should be used in the calculations.

- **Xenon option:** Non-equilibrium for all cases

- **Power density:** Table 4.6 provides the specific power density for each case (40.0 w/gU).
- **Library:** ENDF/B-VII.1
- **Epithermal upscattering:** Both with and without considering epithermal upscattering
- N**umber of depletion zones**
  - UO_2 pellet: 3 equivolumetric zones
  - UO_2+Gd_2O_3 Gadolinia rod: 5 equivolumetric zones
  - WABA & PYREX: 3 equivolumetric zones

4.3.2 Benchmark Results

The benchmark calculations have been performed by using VERA (MPACT+ORIGEN) with the ENDF/B-VII.1 v4.3m1 MPACT 51-group library with and without considering epithermal upscattering and by using the P_2 and TCP_0 scattering options. Reference solutions have been obtained by using the continuous energy Monte Carlo code SERPENT [Lep13] using ENDF/B-VII.1 data. Since SERPENT does not support ENDF/B-VII.1 ACE format library, the Monte Carlo N-Particle (MCNP)-6.1 ACE format library was used with some modification except for on the water S(α,β) data.

Since multiplication factors obtained as a function of burnup are sensitive to neutron flux levels, the same values of recoverable energies per fission have been used for all three codes [Kim16a]. Since there is additional computational burden when using the full ORIGEN burnup chain tracking over 2,200 isotopes, a simplified burnup chain with 255 isotopes was developed to minimize errors in multiplication factors [Kim16a]. Sensitivity calculations were performed using full and simplified burnup chains for all VERA depletion problems. Figure 4.3 provides differences of the multiplication factors in pcm for representative cases. All results with simplified burnup chains except for gadolinia rods are very consistent with those with the full burnup chains, within 50 pcm at all burnup points. Even though the gadolinia rods are the most extreme case showing the largest difference, fuel assemblies with gadolinia rods also show good consistency.

Figures 4.4–4.6 provide comparisons of multiplication factors and pin power distributions as a function of burnup for all benchmark cases considering epithermal upscattering. The VERA calculations have been performed using both P_2 and TCP_0 scattering options. The VERA-CS results with the P_2 scattering option are very consistent with the SERPENT results, within 200 pcm Δk_{eff} at all burnup points, and with 0.5% RMS and 1.0% maximum power difference. The VERA-CS results with the TCP_0 scattering option introduce >200 pcm Δk_{eff} for cases that include control rod insertion and gadolinia burnable poison due to the very anisotropic angular fluxes around very strong neutron absorbers. Figures 4.7–4.9 provide comparisons of multiplication factors and pin power distributions as a function of burnup for all benchmark cases without considering epithermal upscattering. The results are very similar to the benchmark results considering epithermal upscattering.

To see a difference between the ENDF/B-VII.0 and VII.1 libraries for burnup, a sensitivity calculation was performed using SERPENT without considering epithermal upscattering. As shown in Figure 4.10, the ENDF/B-VII.1 library is overestimating the multiplication factors at 30–40 MWD/kgU burnup points by about 100 pcm Δk_{eff}.

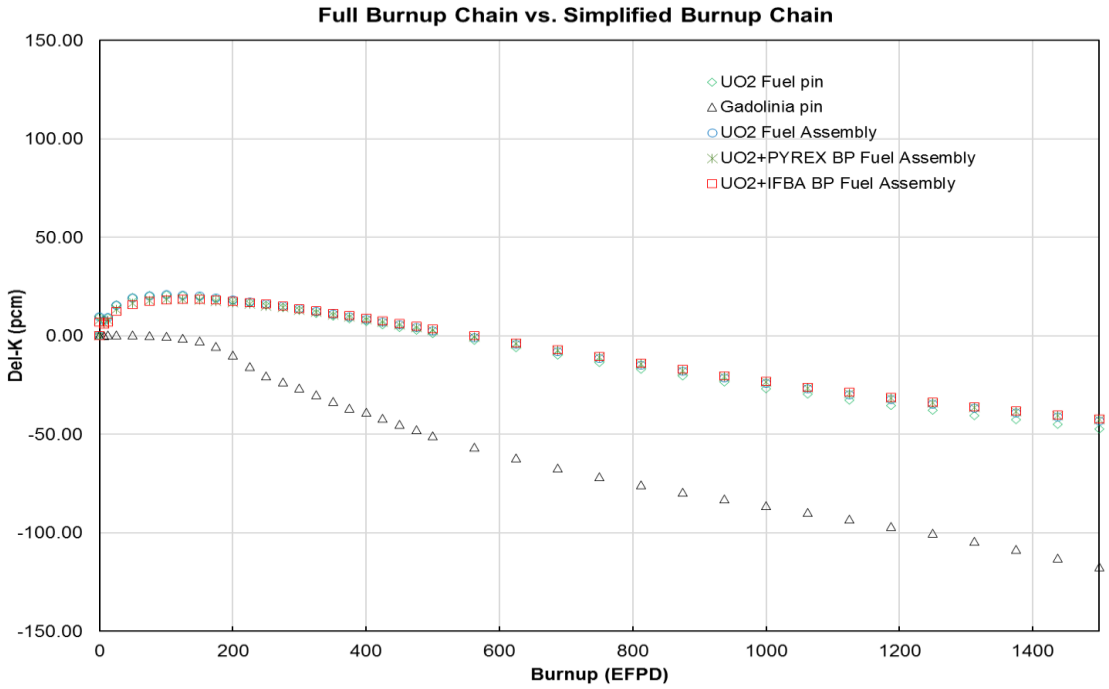

Figure 4.3. Comparison of Simplified Burnup Chain to Full Burnup Chain.

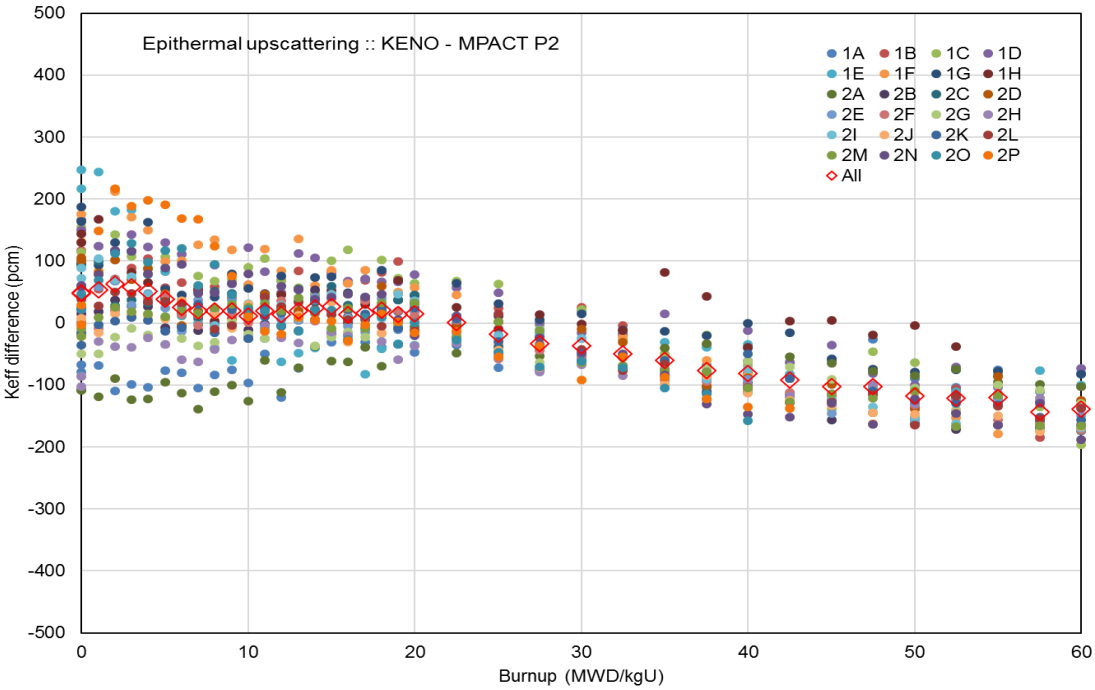

Figure 4.4. Comparison of Multiplication Factors between KENO and MPACT P_2 with Epithermal Upscattering.

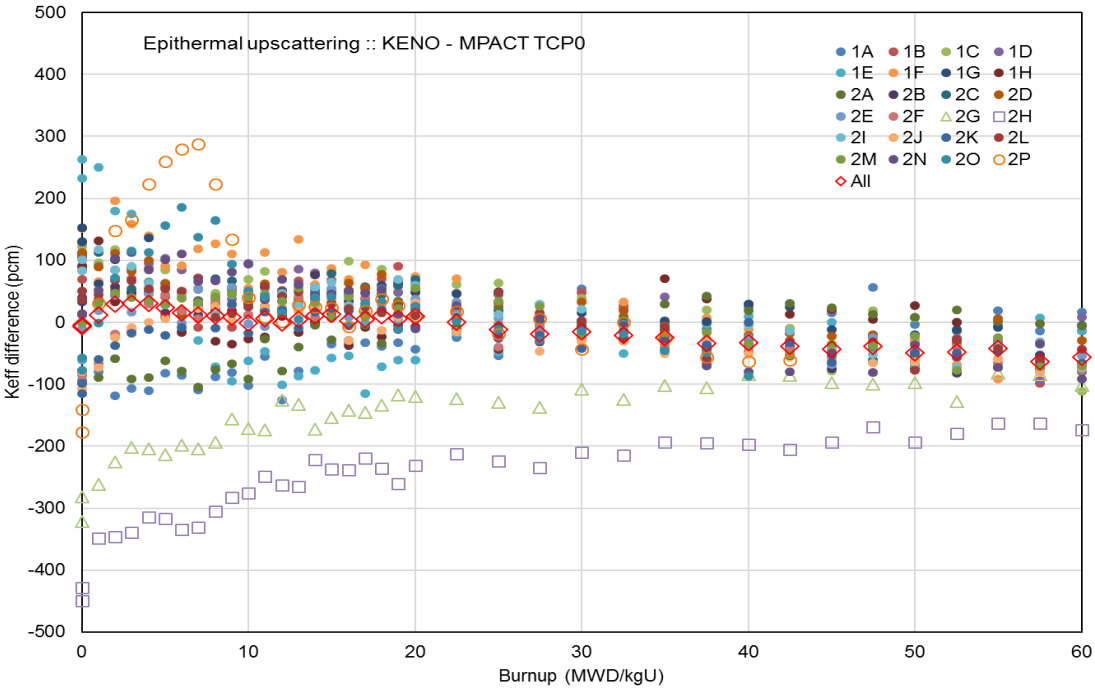

Figure 4.5. Comparison of Multiplication Factors between KENO and MPACT TCP_0 with Epithermal Upscattering.

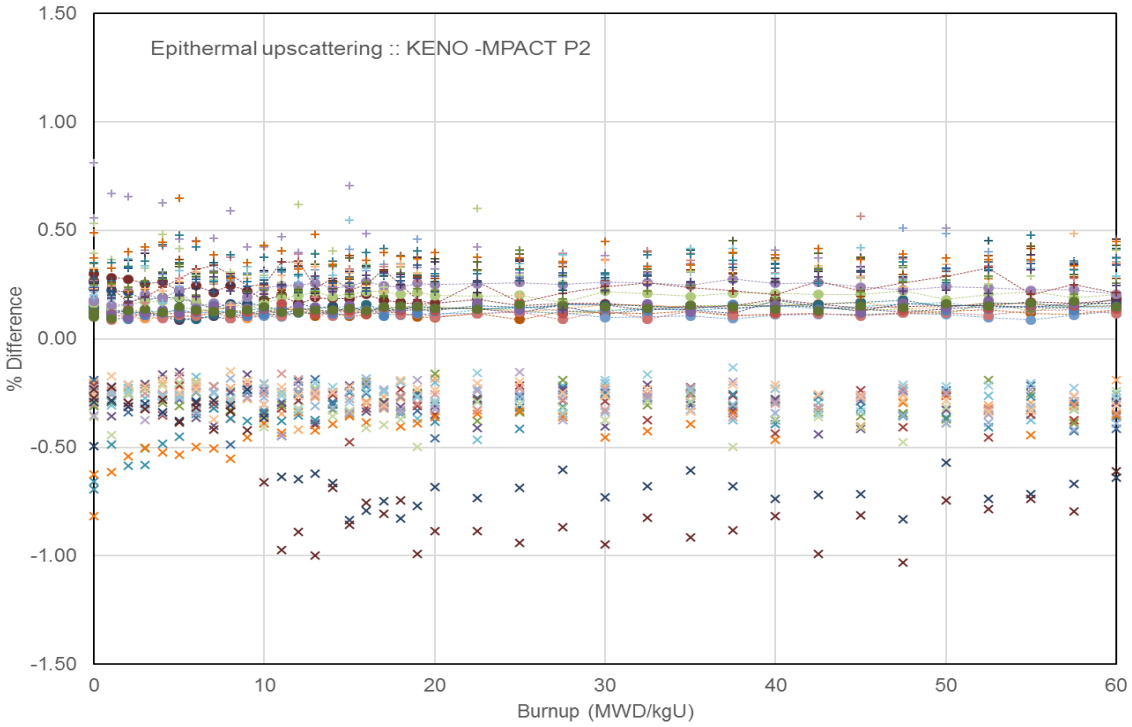

Figure 4.6. Comparison of Pin Powers between KENO and MPACT P_2 with Epithermal Upscattering.

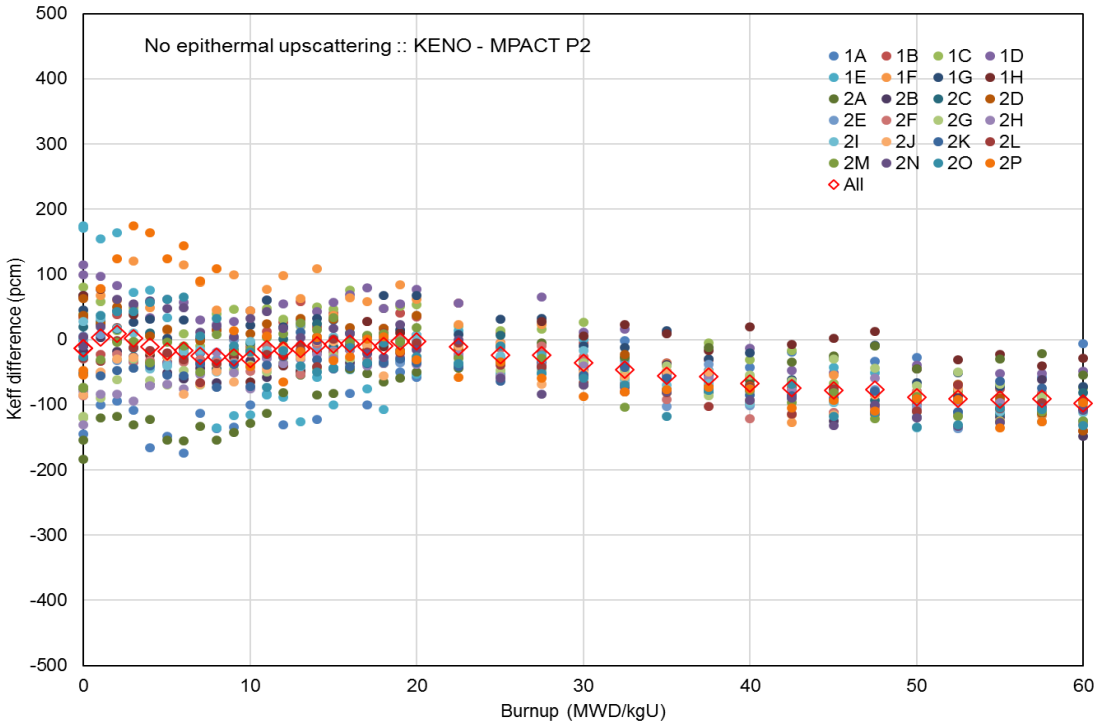

Figure 4.7. Comparison of Multiplication Factors between KENO and MPACT P_2 without Epithermal Upscattering.

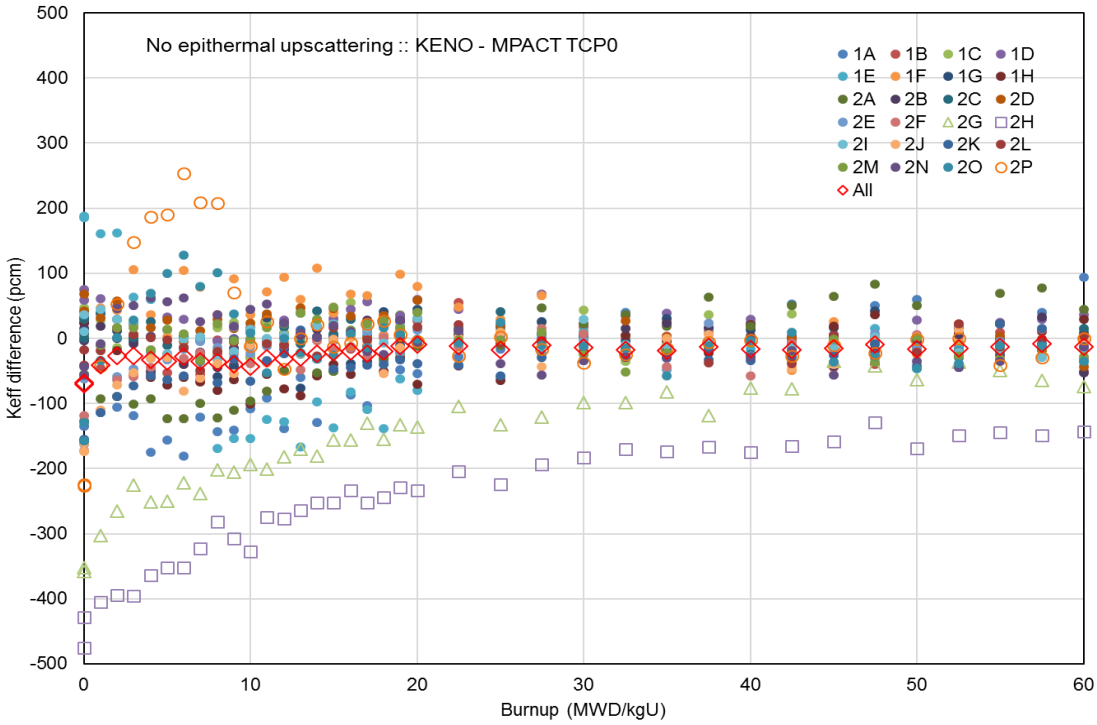

Figure 4.8. Comparison of Multiplication Factors between KENO and MPACT P_2 without Epithermal Upscattering.

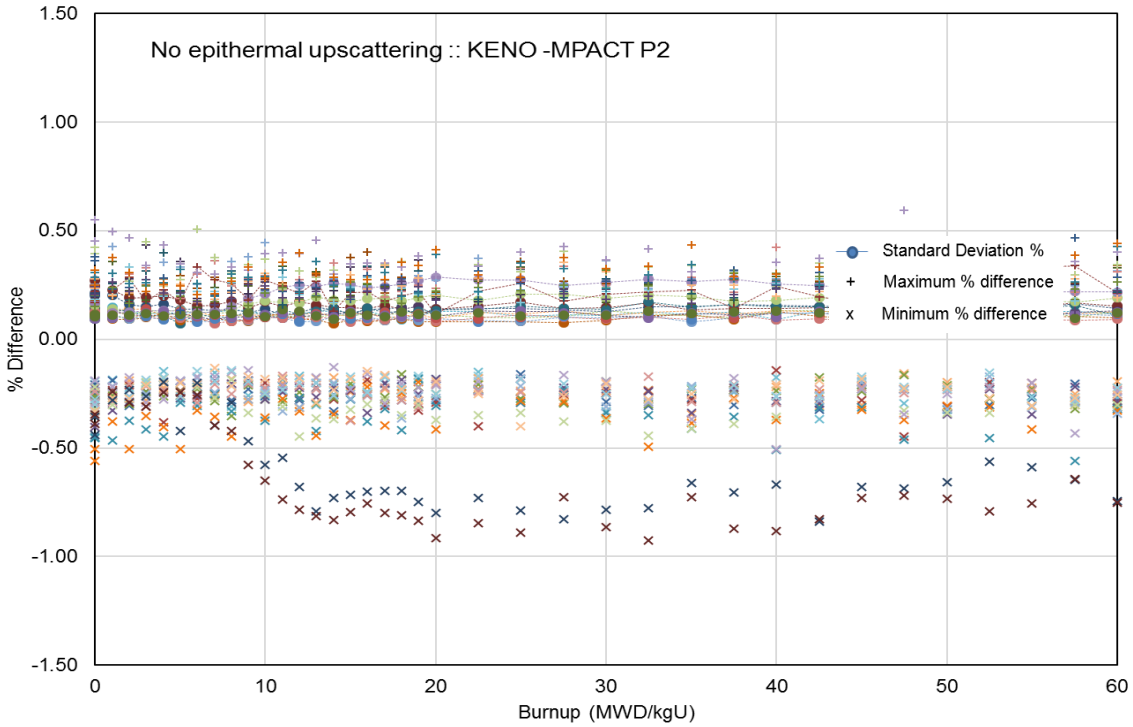

Figure 4.9. Comparison of Pin Powers between KENO and MPACT P_2 without Epithermal Upscattering.

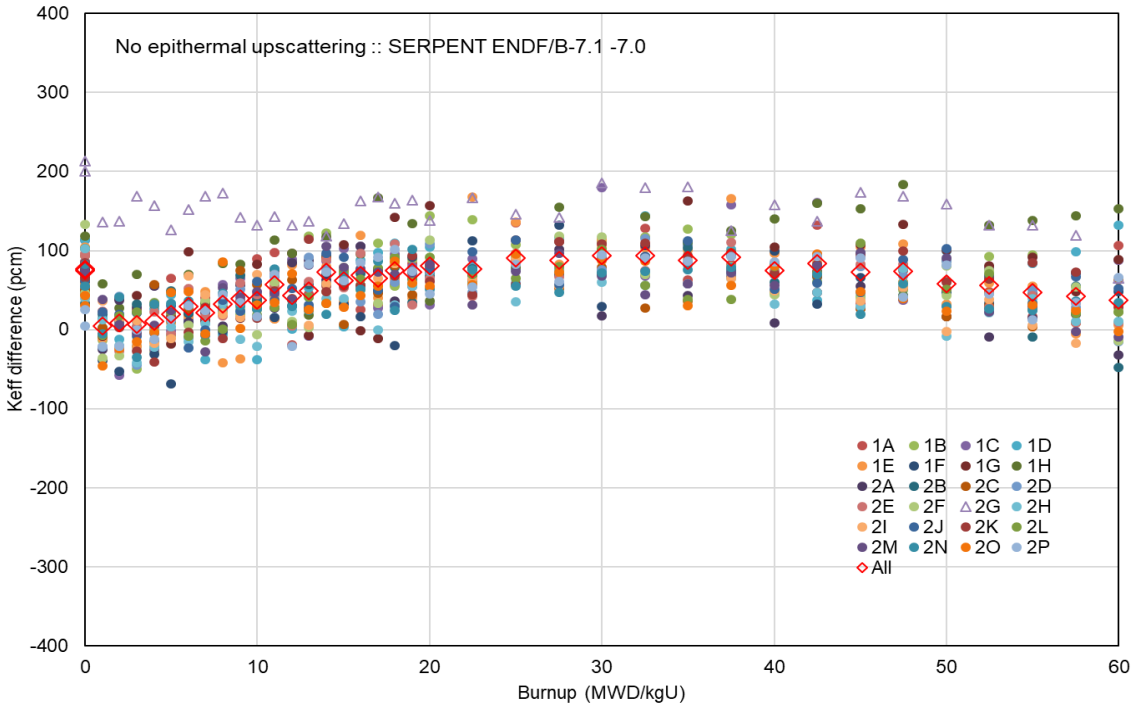

Figure 4.10. Comparison of Multiplication Factors between ENDF/B-VII.0 and ENDF/B-VII.1 using SERPENT without Epithermal Upscattering.

4.4 EXTENSIVE PWR PIN AND ASSEMBLY BENCHMARK PROBLEMS

4.4.1 Characteristics of Problems

Extensive benchmark problems for PWR fuel pins and fuel assemblies have been developed to determine how well the MPACT MG library agrees with continuous-energy Monte Carlo results [Pal17a, Pal17b]. The PWR fuel pin cases consist of:

- 3 ^{235}U enrichments (2.1%, 3.1%, and 4.1%),
- 4 rod sizes corresponding to Watts Bar (WB) Unit 1 Cycle 1 (17 × 17), BEAVRS Cycle 1 (17 × 17), Surry Cycle 1 (15 × 15), and Krsko (16 × 16),
- 3 hot coolant densities corresponding to typical inlet, average, and outlet conditions,
- 3 hot fuel temperatures (600, 900, and 1200K),
- cold cases at room temperature, and
- 3 boron concentrations (0, 600, and 1300 ppm).

There are a total of 360 cases: 324 (3 × 4 × 3 × 3 × 3) hot cases and 36 (3 × 4 × 3) cold cases. The PWR pin cells were modeled as 3 concentric rings of fuel, helium gap, and zirconium surrounded by a square region of coolant. The moderator densities correspond to typical PWR conditions at the core inlet, the core average, and the core outlet. The hot densities are calculated from subcooled steam tables at 2,250 psia. The cold density is at room conditions. Table 4.7 provides moderator temperatures and densities based on various reactor conditions. Table 4.8 provides pin cell dimensions and fuel-to-coolant volume ratios for fuel types. All fuel had a stack density of 10.257 g/cc, and the ^{235}U enrichments are 2.1, 3.1, and 4.1%. The same number densities are used in all rod geometries. In terms of fuel-to-moderator ratios, the BEAVRS rod is the “wettest” configuration, and Krsko is the “driest” configuration.

Table 4.7. Moderator Temperatures and Densities

Reactor Condition	Nomenclature	Temperature (K)	Density (g/cc)
Cold	den0	293.6	1.000000
Hot Inlet	den1	566.0	0.740816
Hot Average	den2	583.9	0.703158
Hot Outlet	den3	601.7	0.655986

Table 4.8. Pin Cell Dimensions

Fuel Type	WB 17 × 17	BEAVRS 17 × 17	Surry 15 × 15	Krsko 16 × 16
Pin Pitch (cm)	1.2600	1.2600	1.4300	1.2319
Fuel Outer Radius (cm)	0.4096	0.39218	0.4647	0.4096
Clad Inner Radius (cm)	0.4180	0.40005	0.4742	0.4180
Clad Outer Radius (cm)	0.4750	0.4572	0.5359	0.4750
Fuel-to-Coolant Ratio	0.6000	0.5190	0.5940	0.6520

Additional benchmark problems have been developed for fourteen different PWR assembly types, including 15 × 15, 16 × 16, and 17 × 17 designs by different fuel

vendors, with many different state point conditions encountered in a reactor. The complete set of assembly geometries is listed in Table 4.9. Each assembly type includes 90 different state points, as follows:

- 3 ^{235}U enrichments (2.1%, 3.1%, and 4.1%)
- 3 hot coolant densities corresponding to typical inlet, average, and outlet conditions
- 3 hot fuel temperatures (600, 900, and 1200K)
- 1 cold case at standard room temperature and density
- 3 boron concentrations (0, 600, and 1300 ppm)

There are a total of 81 hot cases (3 × 3 × 3 × 3) and 9 cold cases (3 × 3) per assembly, for a total of 1,260 cases. The Watts Bar assemblies are slightly modified. The modifications include:

- The cladding material is natural zirconium to reduce the number of isotopes in the MCNP model,
- The enrichment, boron, fuel temperatures, and moderator densities are set by the case matrix (described below), and
- The moderator density inside the guide tubes (GTs) and instrument tube (IT) are set to the core inlet conditions.

The assembly geometry descriptions are given in Table 4.10.

Table 4.9. Assembly Geometry Descriptions

Geometry	Description
ce16	CE 16 × 16 Assembly with large water rods
krsko	Krško Westinghouse 16 × 16
surry	Surry Westinghouse 15 × 15
tmi1	TMI B&W 15 × 15 with 4 gad rods
tmi2	TMI B&W 15 × 15 with no gad
wb2a	Watts Bar 2A 17 × 17
wb2e	Watts Bar 2E 17 × 17 12 Pyrex
wb2f	Watts Bar 2F 17 × 17 24 Pyrex
wb2l	Watts Bar 2L 17 × 17 80 IFBA rods
wb2m	Watts Bar 2M 17 × 17 128 IFBA rods
wb2o	Watts Bar 2O 17 × 17 12 gad rods
wb2p	Watts Bar 2P 17 × 17 24 gad rods
wb2w	Watts Bar 2W 17 × 17 thermally expanded
wb2x	Watts Bar 2X 17 × 17 thermally expanded + zone enrichment

Table 4.10. Assembly dimensions

Type	Fuel Rod (cm)			Guide Tube (cm)			Instrument Tube (cm)		
	Pin Pitch	FA pitch	R_{fuel}	R_{gap}	R_{clad}	R_{in}	R_{out}	R_{in}	R_{out}
CE16	1.28524	20.6400	0.41339	0.42164	0.48514	1.14300	1.24460	1.14300	1.24460
KRSKO	1.23200	19.7180	0.40960	0.41800	0.47500	0.55250	0.59800	0.55250	0.59800
SURRY	1.43000	21.5036	0.46469	0.47422	0.53594	0.61392	0.69012	0.61392	0.69012
TMI1	1.44270	21.8110	0.46950	0.47880	0.54610	0.63245	0.67310	0.56005	0.62610
TMI2	1.44270	21.8110	0.46950	0.47880	0.54610	0.63245	0.67310	0.56005	0.62610
WB2A	1.26000	21.5000	0.40960	0.41800	0.47500	0.56100	0.60200	0.55900	0.60500
WB2E	1.26000	21.5000	0.40960	0.41800	0.47500	0.56100	0.60200	0.55900	0.60500
WB2F	1.26000	21.5000	0.40960	0.41800	0.47500	0.56100	0.60200	0.55900	0.60500
WB2L	1.26000	21.5000	0.40960	0.41800	0.47500	0.56100	0.60200	0.55900	0.60500
WB2M	1.26000	21.5000	0.40960	0.41800	0.47500	0.56100	0.60200	0.55900	0.60500
WB2O	1.26000	21.5000	0.40960	0.41800	0.47500	0.56100	0.60200	0.55900	0.60500
WB2P	1.26000	21.5000	0.40960	0.41800	0.47500	0.56100	0.60200	0.55900	0.60500
WB2W	1.26260	21.6050	0.41208	0.41894	0.47607	0.56226	0.60335	0.56226	0.60335
WB2X	1.26260	21.6050	0.41208	0.41894	0.47607	0.56226	0.60335	0.56226	0.60335

4.4.2 Benchmark Results

Pin cell cases

Tables 4.11 and 4.12 summarize the PWR pin cell eigenvalue comparisons between MPACT and KENO with ENDF/B-VII.1, with and without considering epithermal upscattering. The P_2 scattering option was used in Table 4.11, and the TCP_0 scattering option was used in Table 4.12. All results show the differences between the KENO and MPACT eigenvalues in pcm. Overall, the PWR pin results are acceptable. The average of all 324 hot cases was 1 pcm, with a standard deviation of 63 pcm for the P_2 scattering and -32 pcm with a standard deviation of 65 pcm for the TCP_0 scattering. All of the hot cases were between -138 and +138 pcm for the P_2 scattering and between -167 pcm and +84 pcm for the TCP_0 scattering. The cold cases had a bias of approximately 20–30 pcm compared with the hot cases. The PWR pin cell results are depicted as a histogram in Figures 4.11 and 4.12, which shows that the results closely match a normal distribution.

Table 5.6.5 also shows the hot and cold results averaged over individual parameter subgroups (type, enrichment, boron, moderator density, and fuel temperature). A *subgroup* is defined as a group in which all the cases that have a particular parameter. The averages over subgroups show trends in parameters. When using a criterion of 100 pcm between subgroup differences to define a trend, no trends are observed in geometry, enrichment, boron concentration, or moderator density. A trend was observed in the fuel temperature (a 126 pcm difference from 600–1,200K). There is a -58 pcm bias between hot and cold cases and a 156 pcm trend observed in cold boron cases.

Table 5.6.7 summarizes the PWR pin-cell eigenvalue results for MPACT with the ENDF/B-7.1 v5.0m0 SAMPX 51-g library and MCNP with ENDF/B VII.1.

All results show the differences between the MCNP and MPACT eigenvalues in pcm. The average of all 324 hot cases was 15 pcm, with a standard deviation of 85 pcm. Compared to the MPACT 51-g library, the average has been decreased to 15 pcm from 44, but the standard deviation has been increased by 16 pcm. Even though some of eigenvalue differences are over 200 pcm, reactivity differences are still less than 200 pcm. Cold cases show much better agreement between MCNP and MPACT.

Table 4.11. Benchmark Result for Pin Cell Problems (P_2)

Category			Δk_{eff} Difference (pcm)								Count
			Epithermal Upscattering				No Epithermal Upscattering				
			Average	S. Dev.	Min.	Max.	Average	S. Dev.	Min.	Max.	
Sum	All		1	63	-154	138	1	59	-160	127	360
	Hot		4	61	-138	138	5	57	-122	127	324
	Cold		-29	75	-154	98	-32	76	-160	91	36
Hot	Type	beav	-76	81	-138	0	-68	73	-122	0	81
	Type	krsko	-4	31	-58	54	-5	28	-62	46	81
	Type	WB	60	70	-18	138	56	67	-33	127	81
	Type	surry	36	51	-52	111	36	50	-38	101	81
	Enrich	21	8	69	-138	138	5	63	-122	127	108
	Enrich	31	4	59	-115	114	7	56	-107	107	108
	Enrich	41	-1	54	-110	106	3	51	-110	103	108
	Boron	0	39	69	-64	138	40	67	-52	127	108
	Boron	600	6	53	-90	106	5	49	-85	83	108
	Boron	1300	-33	60	-138	42	-31	54	-122	42	108
	Density	den1	0	58	-132	118	1	56	-122	113	108
	Density	den2	3	62	-138	131	5	57	-115	115	108
	Density	den3	8	64	-132	138	9	58	-120	127	108
	Tfuel	600	-4	57	-138	118	-4	54	-122	97	108
	Tfuel	900	7	61	-117	138	9	57	-115	119	108
	Tfuel	1200	8	66	-132	131	9	60	-120	127	108
Cold	Type	Beav	-69	87	-138	6	-70	87	-141	5	9
	Type	Krsko	-9	51	-75	70	-13	55	-88	60	9
	Type	WB	-38	92	-154	76	-45	93	-160	63	9
	Type	Surry	0	64	-87	98	1	61	-74	91	9
	Enrich	21	-23	81	-154	98	-28	82	-160	91	12
	Enrich	31	-33	75	-143	68	-35	76	-139	78	12
	Enrich	41	-31	70	-135	59	-33	70	-133	63	12
	Boron	0	46	57	-13	98	44	54	-18	91	12
	Boron	600	-27	39	-69	16	-33	44	-79	7	12
	Boron	1300	-106	111	-154	0	-107	112	-160	0	12

Table 4.12. Benchmark Result for Pin Cell Problems (TCP_0)

Category			Δk_{eff} Difference (pcm)								Count
			Epithermal Upscattering				No Epithermal Upscattering				
			Average	S. Dev.	Min.	Max.	Average	S. Dev.	Min.	Max.	
Sum	All		-32	65	-167	93	-33	62	-157	84	360
	Hot		-34	66	-167	84	-35	63	-157	66	324
	Cold		-15	54	-108	93	-20	55	-116	84	36
Hot	Type	beav	-109	111	-167	0	-103	105	-157	0	81
	Type	krsko	-49	54	-92	0	-51	55	-90	0	81
	Type	WB	23	35	-28	84	18	31	-45	66	81
	Type	surry	-1	28	-71	60	-2	26	-57	47	81
	Enrich	21	-29	70	-167	84	-34	67	-157	66	108
	Enrich	31	-34	64	-144	59	-33	61	-143	59	108
	Enrich	41	-40	64	-144	46	-37	60	-129	44	108
	Boron	0	-10	57	-118	84	-11	53	-102	66	108
	Boron	600	-33	61	-128	56	-35	59	-125	41	108
	Boron	1300	-60	77	-167	11	-59	73	-157	8	108
	Density	den1	-32	62	-151	70	-33	60	-132	64	108
	Density	den2	-34	67	-153	78	-34	62	-143	66	108
	Density	den3	-36	69	-167	84	-37	65	-157	65	108
	Tfuel	600	-36	63	-153	69	-38	62	-132	57	108
	Tfuel	900	-31	64	-144	84	-30	60	-130	66	108
	Tfuel	1200	-36	70	-167	78	-36	66	-157	65	108
Cold	Type	Beav	-50	60	-96	4	-52	61	-93	2	9
	Type	Krsko	-5	34	-51	57	-10	39	-66	45	9
	Type	WB	-22	68	-108	71	-31	70	-116	56	9
	Type	Surry	15	50	-56	93	13	46	-42	84	9
	Enrich	21	-5	59	-108	93	-12	59	-116	84	12
	Enrich	31	-20	54	-104	60	-24	55	-102	68	12
	Enrich	41	-22	50	-96	48	-25	51	-100	51	12
	Boron	0	37	50	-19	93	33	46	-26	84	12
	Boron	600	-14	29	-54	34	-22	34	-58	23	12
	Boron	1300	-69	75	-108	0	-72	77	-116	0	12

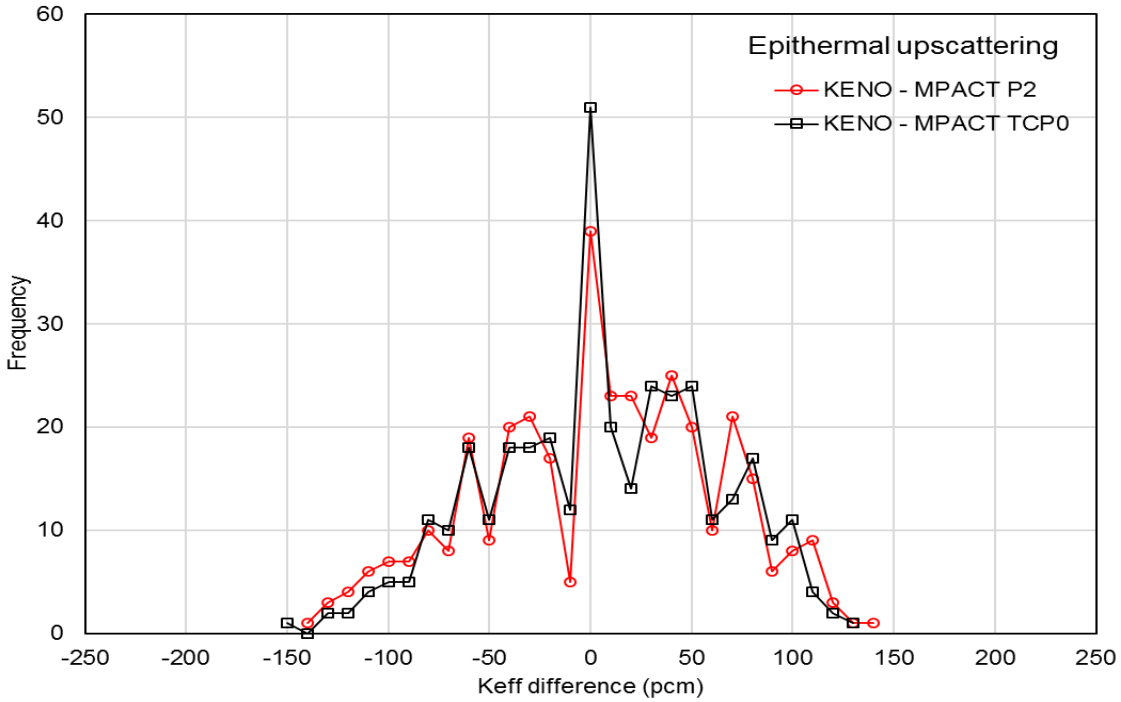

Figure 4.11. Pin k_{eff} Difference Distribution with Epithermal Upscattering.

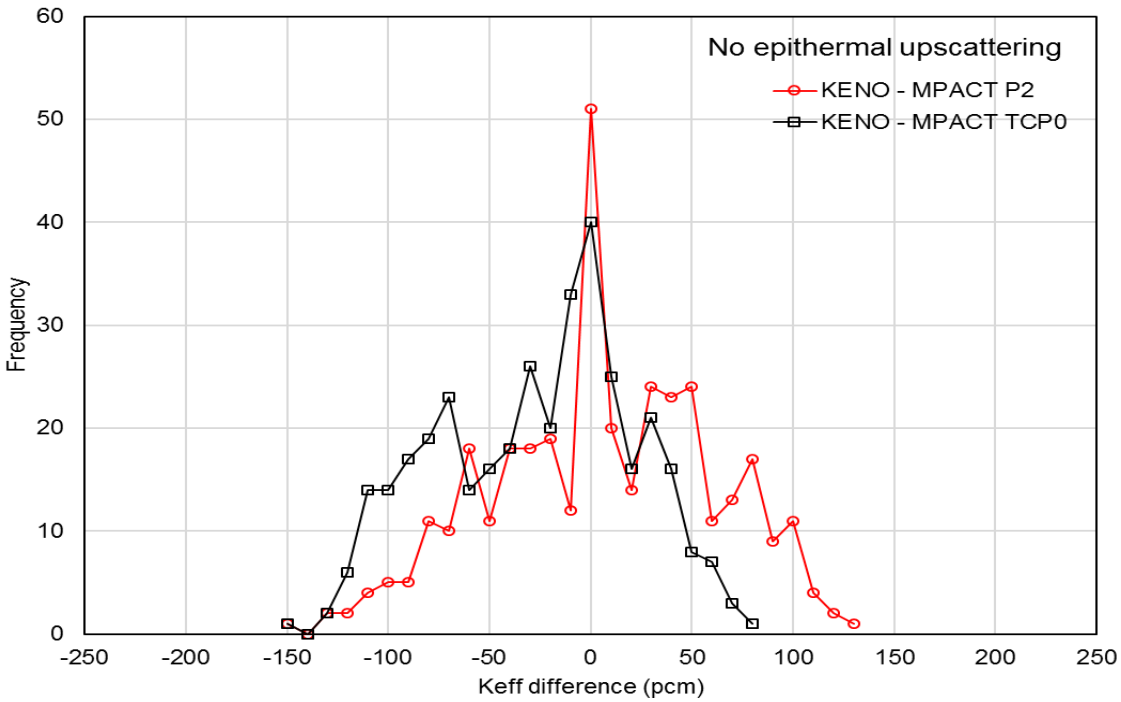

Figure 4.12. Pin k_{eff} Difference Distribution without Epithermal Upscattering.

Assembly cases

Tables 4.13 and 4.14 summarize PWR assembly benchmark results with and without considering epithermal upscattering and with the P_2 scattering. Overall, the eigenvalue results are acceptable. The averages of all 1,134 hot cases are -7 pcm, with a standard deviation of 54 pcm for the epithermal upscattering and -6 pcm with a standard deviation of 52 pcm without epithermal upscattering.

All of the hot cases are between -192 and +126 pcm for the epithermal upscattering and between -180 pcm and 118 pcm without epithermal upscattering. A reasonable goal is to have all eigenvalue differences between +/- 200 pcm. Standard deviations of the cold cases are about 140 pcm for both cases, which are much larger compared to the hot cases. The hot pin power results look very good. All of the hot assemblies have a maximum pin power less than 0.5%. The cold pin power results are not as good, and the maximum error is almost 1%. Additional coolant rings may need to be included in the cold cases to reduce the maximum pin power errors.

Some cases have very large cold eigenvalue differences. For example, the high gad case (wb2p) at low enrichments has a maximum eigenvalue difference of -568 pcm. This large maximum is not observable in the hot cases. The largest cold pin power differences are in the CE16 assemblies, which have the large water rods. The larger pin power differences in cold cases may be due to not modeling enough rings (at source regions) in the coolant. This is more important for cold cases, which have higher moderator densities than the hot cases. The eigenvalue results over all cases are shown as histograms in Figures 4.13 and 4.14.

Reference solution and scattering order

The reference solutions for this benchmark suite were obtained using KENO and MCNP. However, the MPACT MG libraries have been developed to be consistent with the CE-KENO results, for which the SPH factors were obtained by performing the CE-KENO calculations. Figure 4.14 shows an intrinsic difference between MCNP and CE-KENO, for which the k_{eff} differences are between -180 pcm and 160 pcm.

In these benchmark calculations, the MPACT calculations were also performed by the TCP0 option, which is a default option for power plant simulation. The ^{1}H transport cross sections were developed to accurately consider neutron leakage for large size problems. Therefore, when developing the cross section library and performing the small size problem, a high order scattering ($\geq P_2$) calculation would be more reasonable. The TCP_0 results get closer to the P_2 results as the problem size increases.

Table 4.13 Benchmark Result for Assembly Problems with Epithermal Upscattering

	Category		Δk_{eff} Difference (pcm)				Pin Power Diff. %		Count
			Average	S. Dev.	Min.	Max.	Ave. RMS	Max. Pin	
Sum	Total All		-6	67	-240	568	0.11	0.93	1260
	Total Hot		-7	54	-192	126	0.10	0.47	1134
	Total Cold		-4	138	-240	568	0.23	0.93	126
Hot	Type	ce16	22	43	-51	122	0.09	0.26	81
	Type	krsko	14	45	-78	108	0.09	0.37	81
	Type	surry	38	53	-44	126	0.07	0.24	81
	Type	tmi1	34	51	-48	126	0.10	0.47	81
	Type	tmi2	47	57	-17	115	0.09	0.25	81
	Type	wb2a	6	38	-79	82	0.09	0.30	81
	Type	wb2e	-16	42	-81	93	0.07	0.24	81
	Type	wb2f	-49	60	-110	40	0.11	0.32	81
	Type	wb2l	-36	49	-116	31	0.09	0.29	81
	Type	wb2m	-102	108	-192	0	0.10	0.27	81
	Type	wb2o	-24	47	-110	65	0.14	0.45	81
	Type	wb2p	-34	51	-118	59	0.16	0.42	81
	Type	wb2w	5	37	-76	79	0.08	0.28	81
	Type	wb2x	4	37	-79	79	0.08	0.27	81
	Enrich	21	12	54	-156	126	0.09	0.45	378
	Enrich	31	-11	54	-192	109	0.10	0.41	378
	Enrich	41	-21	54	-170	91	0.10	0.47	378
	Boron	0	1	62	-192	126	0.10	0.45	378
	Boron	600	-6	48	-154	88	0.10	0.46	378
	Boron	1300	-14	51	-170	126	0.09	0.47	378
	Density	den1	10	53	-170	126	0.10	0.46	378
	Density	den2	0	44	-126	86	0.10	0.46	378
	Density	den3	-30	63	-192	126	0.10	0.47	378
	Tfuel	600	-14	53	-179	117	0.10	0.45	378
	Tfuel	900	-4	54	-192	126	0.10	0.46	378
	Tfuel	1200	-3	55	-168	119	0.10	0.47	378
Cold	Type	ce16	-110	143	-240	16	0.28	0.93	9
	Type	krsko	-20	70	-108	80	0.21	0.66	9
	Type	surry	-86	127	-204	43	0.23	0.46	9
	Type	tmi1	-35	98	-154	111	0.27	0.62	9
	Type	tmi2	-79	121	-212	49	0.23	0.51	9
	Type	wb2a	-58	98	-172	53	0.21	0.47	9
	Type	wb2e	69	117	-60	242	0.21	0.58	9
	Type	wb2f	147	186	0	389	0.21	0.76	9
	Type	wb2l	-35	95	-158	110	0.2	0.65	9
	Type	wb2m	-71	119	-220	101	0.14	0.5	9
	Type	wb2o	98	149	-55	315	0.26	0.65	9
	Type	wb2p	237	286	0	568	0.3	0.8	9
	Type	wb2w	-55	93	-150	55	0.21	0.47	9
	Type	wb2x	-57	96	-162	53	0.21	0.47	9
	Enrich	21	34	175	-240	568	0.22	0.77	42
	Enrich	31	-15	127	-217	348	0.23	0.84	42
	Enrich	41	-31	104	-220	237	0.23	0.93	42
	Boron	0	101	157	-21	568	0.26	0.93	42
	Boron	600	-5	108	-119	361	0.23	0.76	42
	Boron	1300	-108	146	-240	183	0.2	0.66	42

Table 4.14 Benchmark Result for Assembly Problems without Epithermal Upscattering

	Category		Δk_{eff} Difference (pcm)				Pin Power Diff. %		Count
			Average	S. Dev.	Min.	Max.	Ave. RMS	Max. Pin	
Sum	Total All		-6	66	-237	571	0.11	0.93	1260
	Total Hot		-6	52	-180	118	0.10	0.47	1134
	Total Cold		-7	139	-237	571	0.23	0.93	126
Hot	Type	ce16	23	43	-50	118	0.09	0.26	81
	Type	krsko	17	44	-79	95	0.09	0.37	81
	Type	surry	32	47	-47	117	0.07	0.24	81
	Type	tmi1	26	44	-51	107	0.10	0.47	81
	Type	tmi2	41	52	-36	108	0.09	0.25	81
	Type	wb2a	7	37	-68	79	0.09	0.30	81
	Type	wb2e	-15	41	-88	91	0.07	0.24	81
	Type	wb2f	-45	58	-109	59	0.11	0.32	81
	Type	wb2l	-34	47	-101	38	0.09	0.29	81
	Type	wb2m	-98	104	-180	0	0.10	0.27	81
	Type	wb2o	-18	43	-109	73	0.14	0.45	81
	Type	wb2p	-31	50	-127	57	0.16	0.42	81
	Type	wb2w	6	37	-75	84	0.08	0.28	81
	Type	wb2x	8	37	-77	84	0.08	0.27	81
	Enrich	21	10	51	-143	118	0.09	0.45	378
	Enrich	31	-10	52	-180	95	0.10	0.41	378
	Enrich	41	-18	52	-178	87	0.10	0.47	378
	Boron	0	1	60	-180	108	0.10	0.45	378
	Boron	600	-6	45	-171	73	0.10	0.46	378
	Boron	1300	-13	48	-143	118	0.09	0.47	378
	Density	den1	10	51	-143	108	0.10	0.46	378
	Density	den2	2	41	-120	78	0.10	0.46	378
	Density	den3	-29	61	-180	118	0.10	0.47	378
	Tfuel	600	-14	52	-171	107	0.10	0.45	378
	Tfuel	900	-1	50	-169	118	0.10	0.46	378
	Tfuel	1200	-3	53	-180	117	0.10	0.47	378
Cold	Type	ce16	-110	144	-237	18	0.28	0.93	9
	Type	krsko	-28	80	-132	78	0.21	0.66	9
	Type	surry	-89	130	-221	34	0.23	0.46	9
	Type	tmi1	-44	108	-163	109	0.27	0.62	9
	Type	tmi2	-77	117	-203	43	0.23	0.51	9
	Type	wb2a	-55	92	-154	52	0.21	0.47	9
	Type	wb2e	60	103	-65	211	0.21	0.58	9
	Type	wb2f	150	194	-20	409	0.21	0.76	9
	Type	wb2l	-36	94	-153	122	0.2	0.65	9
	Type	wb2m	-74	113	-212	78	0.14	0.5	9
	Type	wb2o	90	145	-69	304	0.26	0.65	9
	Type	wb2p	234	285	0	571	0.3	0.8	9
	Type	wb2w	-59	97	-168	46	0.21	0.47	9
	Type	wb2x	-61	100	-170	46	0.21	0.47	9
	Enrich	21	32	176	-237	571	0.22	0.77	42
	Enrich	31	-18	127	-226	350	0.23	0.84	42
	Enrich	41	-35	103	-212	212	0.23	0.93	42
	Boron	0	98	156	-28	571	0.26	0.93	42
	Boron	600	-8	108	-117	373	0.23	0.76	42
	Boron	1300	-111	148	-237	181	0.2	0.66	42

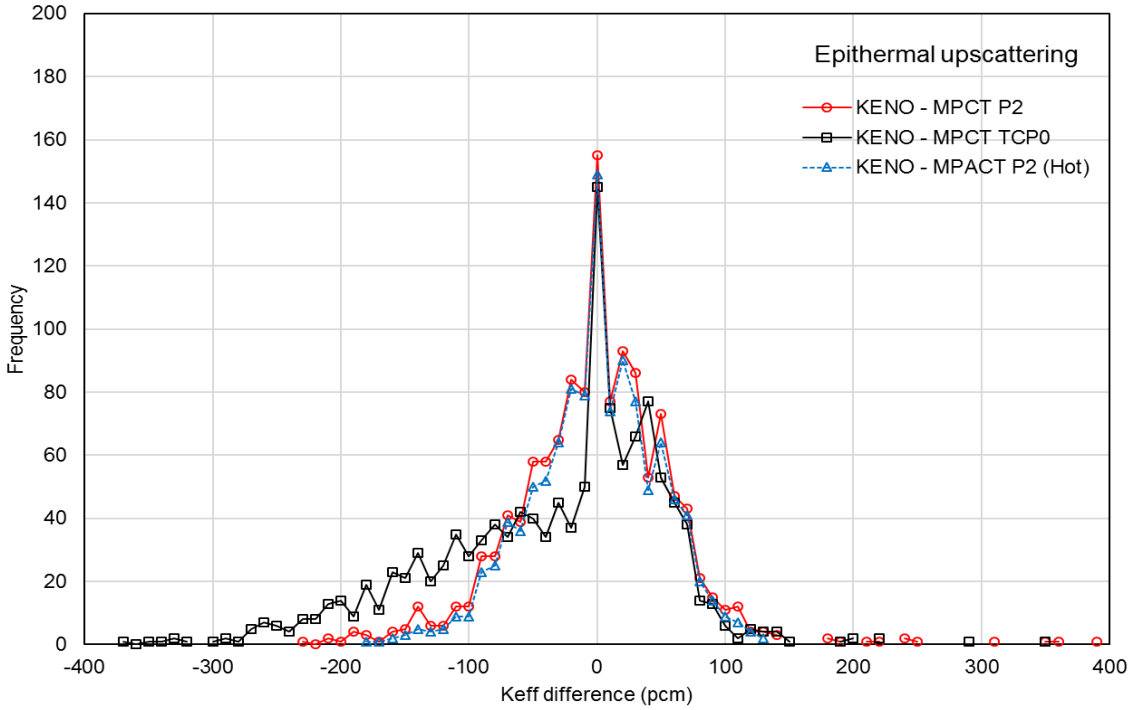

Figure 4.13. Assembly k_{eff} Difference Distribution with Epithermal Upscattering.

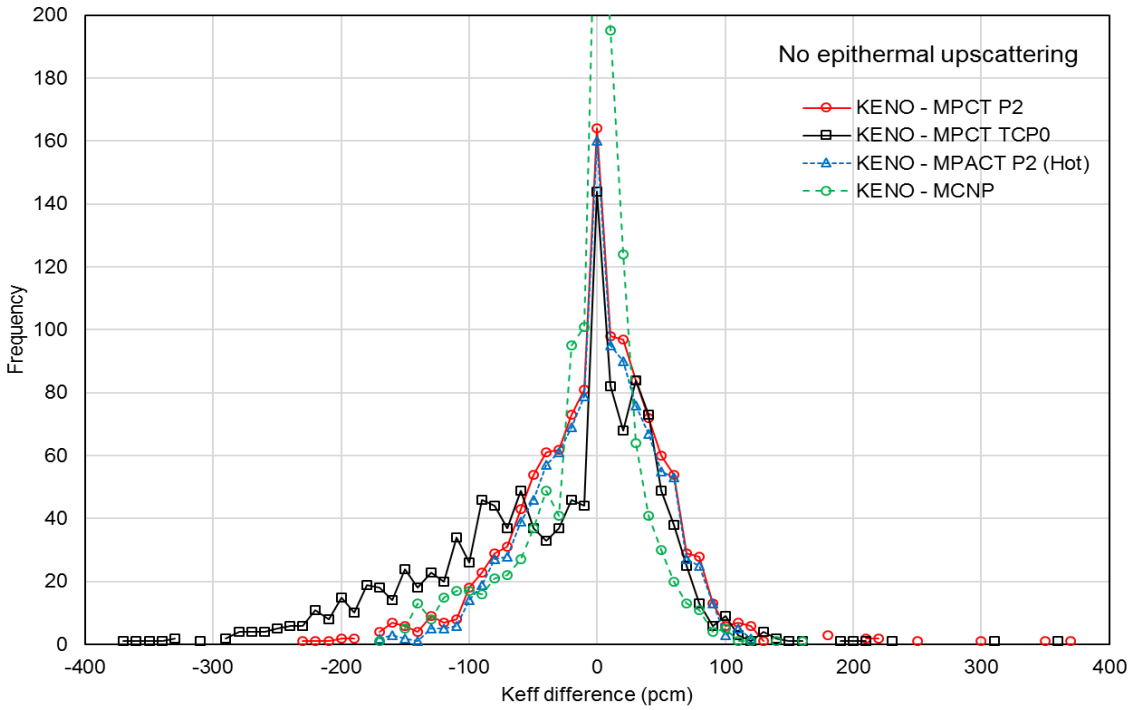

Figure 4.14. Assembly k_{eff} Difference Distribution without Epithermal Upscattering.

4.5 NONUNIFORM FUEL TEMPERATURE BENCHMARK PROBLEMS

4.5.1 Characteristics of Problems

Seoul National University (SNU) has developed a benchmark suite for the intra-pellet nonuniform temperature distribution cases [Joo05]. Table 4.15 and Figure 4.16 provide the geometrical specifications, including five equivolume subzones in the fuel pellet, gap, cladding, and moderator. Table 4.16 provides the compositional specification, including nuclides and atomic number densities.

Nonuniform temperature profiles as a function of power and average fuel temperatures are shown in Table 4.17 and Figure 4.15. Benchmark calculations are performed by using both nonuniform and uniform temperature profiles.

Table 4.15. Geometrical Data

Region	Dimensions		
Fuel	Outer Radius (cm)		0.4127
	Sub-pellet annular ring radius (cm)	1	0.1846
		2	0.2610
		3	0.3197
		4	0.3692
		5	0.4127
Gap			
Clad	Inner Radius (cm)		0.4203
	Outer Radius (cm)		0.4862
Coolant	Cell Pitch (cm)		1.2870

Table 4.16. Composition Data

Composition	Nuclides		Atomic Number Density (atoms/barn-cm)
3.0% UO_2	^{235}U	92,235	7.13479E-04
	^{238}U	92,238	2.27778E-02
	^{16}O	8,016	4.69825E-02
Gap	^{16}O	8,016	1.00000E-08
Clad	^{90}Zr	40,090	2.22157E-02
	^{91}Zr	40,091	4.79136E-03
	^{92}Zr	40,092	7.24405E-03
	^{94}Zr	40,094	7.18475E-03
	^{96}Zr	40,096	1.13334E-03
Coolant	^{1}H	1,001	4.65690E-02
	^{16}O	8,016	2.32840E-02

Table 4.17. Nonuniform Temperature Profiles as a Function Power

Region		Temperature (K) Power Level (%)						
		50	75	100	125	150	175	200
Pellet	1	787.4	897.7	1017.9	1148.2	1288.2	1437.7	1596.3
	2	754.7	843.7	939.3	1041.7	1150.6	1266.0	1387.5
	3	723.1	792.2	865.1	942.0	1022.7	1107.3	1195.6
	4	683.0	728.3	774.9	823.2	873.0	924.3	977.1
	5	669.2	708.3	748.4	789.4	831.4	874.3	918.2
	Avg.	723.5	794.0	869.1	948.9	1033.2	1121.9	1214.9
Gap		606.1	610.2	614.0	617.7	621.2	624.7	628.1
Clad		606.1	610.2	614.0	617.7	621.2	624.7	628.1
Coolant		586.7	586.7	586.7	586.7	586.7	586.7	586.7

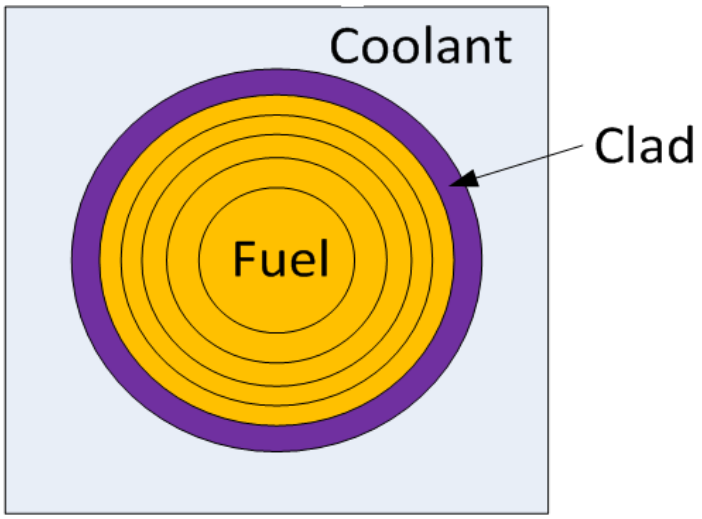

Figure 4.15. Geometrical Configuration.

4.5.2 Benchmark Results

Benchmark calculations were performed using the continuous-energy Monte Carlo code KENO using the ENDF/B-VII.1 nuclear data and the VERA-CS MPACT using the ENDF/B-VII.1 v4.3m1 MPACT 51-group library. SCALE-6.2 with CE-KENO includes a new capability to interpolate continuous-energy cross sections for any specified temperature based on the reference temperatures for base cross sections.

Figure 4.16 provides a comparison of reactivities between nonuniform and uniform temperature profile results obtained by KENO. This comparison indicates that the slopes of nonuniform and uniform temperature profiles, which determine the fuel temperature reactivity coefficient, are different. In other words, the fuel temperature coefficient of the nonuniform temperature is less negative than that of the uniform temperature. Therefore, when performing whole core calculations with thermal/hydraulic

(T/H) feedback, nonuniform temperature profiles must be considered properly in estimating resonance self-shielded cross sections by performing subgroup calculations.

Figure 4.17 provides the benchmark results for the uniform temperature cases. There are very good agreements between the KENO and the MPACT results, with both P_2 and TCP_0 scatterings in the reactivities for all temperatures. Figure 4.18 provides the benchmark results for the nonuniform temperature cases. There are very good agreements between the KENO and the MPACT results, with both P_2 and TCP_0 scatterings in the reactivities for all temperatures.

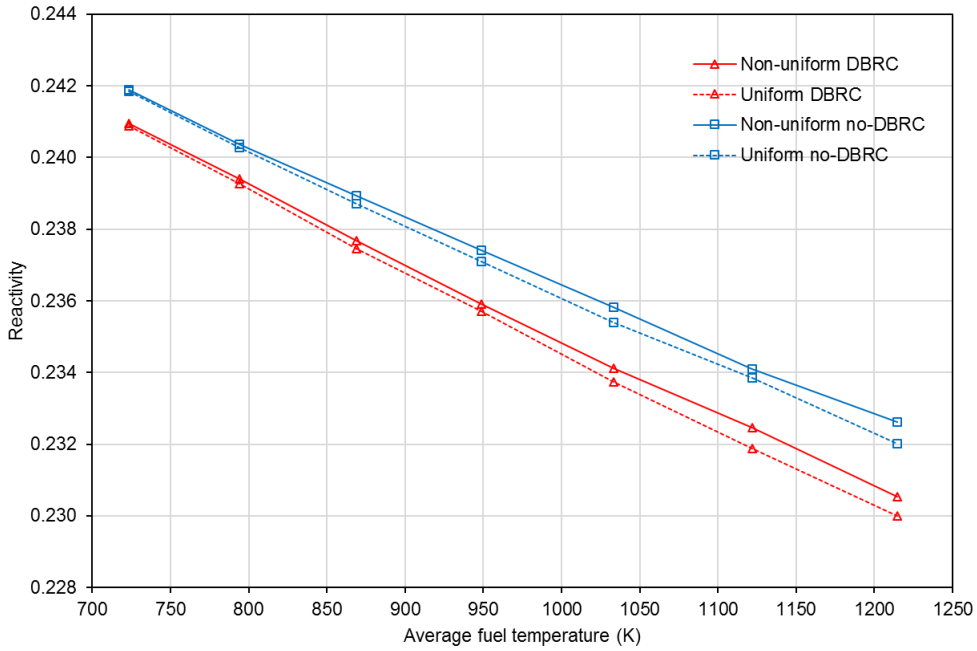

Figure 4.16. Comparison of Reactivities between Nonuniform and Uniform Temperature Distributions. (KENO).

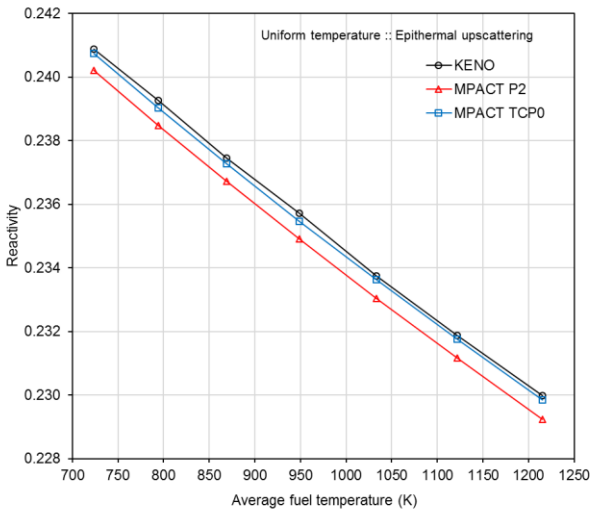

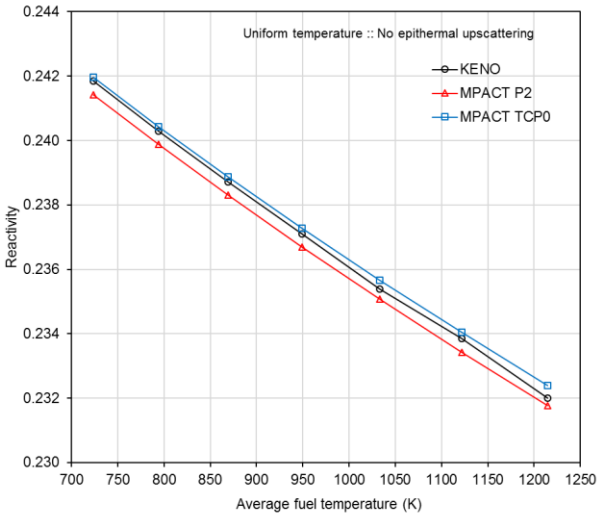

Code	Epithermal Upscattering		No Epithermal Upscattering	
	FTC (pcm/K)	ΔFTC (pcm/K)	FTC (pcm/K)	ΔFTC (pcm/K)
KENO[a]	2.22		2.01	
MPACT P_2[b]	2.25	-0.03	1.98	0.03
MPACT TCP_0[b]	2.23	-0.02	1.96	0.05

Figure 4.17. Comparison of Reactivities for the Uniform Temperature Distributions.

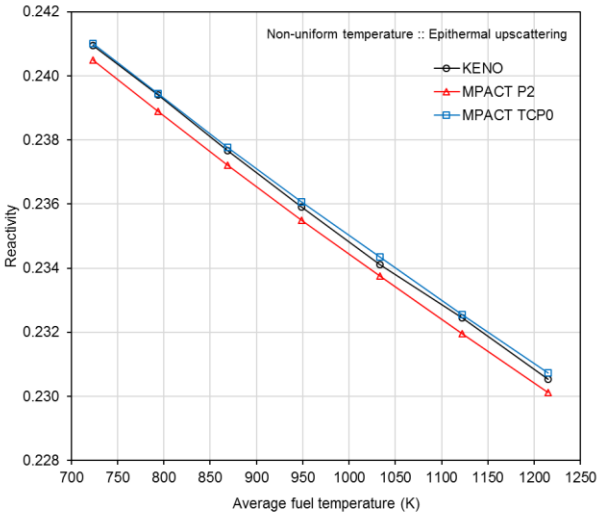

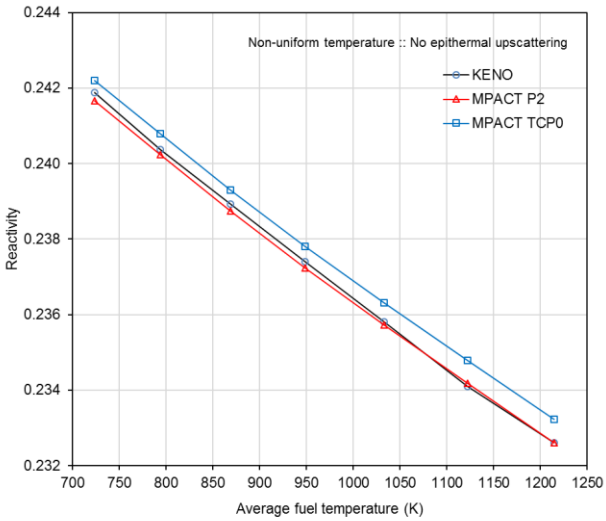

Code	Epithermal Upscattering		No Epithermal Upscattering	
	FTC (pcm/K)	ΔFTC (pcm/K)	FTC (pcm/K)	ΔFTC (pcm/K)
KENO[a]	2.13	-	1.90	-
MPACT P_2[b]	2.12	0.01	1.86	0.04
MPACT TCP_0[b]	2.10	0.03	1.84	0.06

Figure 4.18. Comparison of Reactivities for the Nonuniform Temperature Distributions.

4.6 MOSTELLER BENCHMARK PROBLEMS

4.6.1 Characteristics of Problems

The Mosteller benchmark [Mos07] was developed to verify the Doppler temperature reactivity coefficient. Tables 4.18–4.20 provide the compositional and geometrical specifications. The original benchmarks do not include 1,200K cases, which have been added to these benchmark calculations.

Table 4.18. Atomic Number Densities of UO_2 Fuels

Temp (K)	Nuclide	Atomic Number Density vs ^{235}U Enrichment						
		0.711	1.6	2.4	3.1	3.9	4.5	5.0
600	^{16}O	4.61171E-02	4.61218E-02	4.61260E-02	4.61297E-02	4.61339E-02	4.61371E-02	4.61397E-02
	^{234}U	0.00000E+00	3.00175E-06	4.50257E-06	5.81576E-06	7.31651E-06	8.44205E-06	9.37998E-06
	^{235}U	1.66029E-04	3.73618E-04	5.60420E-04	7.23867E-04	9.10661E-04	1.05075E-03	1.16749E-03
	^{238}U	2.28925E-02	2.26843E-02	2.24981E-02	2.23352E-02	2.21490E-02	2.20093E-02	2.18930E-02
900	^{16}O	4.59967E-02	4.60014E-02	4.60056E-02	4.60093E-02	4.60134E-02	4.60166E-02	4.60192E-02
	^{234}U	0.00000E+00	2.99391E-06	4.49081E-06	5.80057E-06	7.29740E-06	8.42000E-06	9.35548E-06
	^{235}U	1.65595E-04	3.72642E-04	5.58956E-04	7.21977E-04	9.08283E-04	1.04801E-03	1.16445E-03
	^{238}U	2.28328E-02	2.26251E-02	2.24393E-02	2.22768E-02	2.20911E-02	2.19519E-02	2.18358E-02
1200	^{16}O	4.58763E-02	4.58810E-02	4.58852E-02	4.58889E-02	4.58929E-02	4.58961E-02	4.58987E-02
	^{234}U	0.00000E+00	2.98607E-06	4.47905E-06	5.78538E-06	7.27829E-06	8.39795E-06	9.33098E-06
	^{235}U	1.65161E-04	3.71666E-04	5.57492E-04	7.20087E-04	9.05905E-04	1.04527E-03	1.16141E-03
	^{238}U	2.27731E-02	2.25659E-02	2.23805E-02	2.22184E-02	2.20332E-02	2.18945E-02	2.17786E-02

Table 4.19. Geometrical Configurations

	600K	900K	1200K
Fuel outer radius(cm)	0.39398	0.39433	0.39468
Clad inner radius (cm)	0.40226	0.40226	0.40226
Clad outer radius (cm)	0.45972	0.45972	0.45972
Pin pitch (cm)	1.26678	1.26678	1.26678

Table 4.20. Atomic Number Densities of Moderator and Clad

Material	Temp	Atomic number density					
Moderator	600	1001	4.42326E-02	8016	2.21163E-02	5010	1.02133E-05
		5011	4.11098E-05				
Clad	600	40090	2.17036E-02	40091	4.73302E-03	40092	7.23452E-03
		40094	7.33155E-03	40096	1.18115E-03		
Gap	600	8016	2.68714E-05				

4.6.2 Benchmark Results

Benchmark calculations were performed using the continuous-energy Monte Carlo codes KENO and MCNP using the ENDF/B-VII.1 nuclear data and the VERA-CS MPACT using the ENDF/B-VII.1 v4.3m1 MPACT 51-group library.

Table 4.21 and Figures 4.19 and 4.20 provide the benchmark results with and without considering epithermal upscattering. The P_2 MPACT results are consistent with the KENO results within 100 pcm with both options with and without epithermal and

upscattering. Though the TCP_0 MPACT results are slightly worse than the P_2 results, the maximum differences are still less than 117 pcm. Figures 4.19 and 4.20 show very good agreement between the MPACT and Monte Carlo results at any temperature range. It is noted that the ENDF/B-VII.1 v4.3m1 MPACT 51-group library does not include any Doppler temperature reactivity bias.

Table 4.21. Benchmark Results for Mosteller

^{235}U wgt%	Temp.(K)	Epithermal upscattering			No epithermal upscattering			
		KENO	Δk (pcm)		KENO	Δk (pcm)		
			P_2	TCP_0		MCNP	P_2	TCP_0
0.711	600	0.66515	-16	-16	0.66594	31	-17	-18
	900	0.65878	-15	-18	0.66020	5	-29	-34
	1,200	0.65317	-4	-10	0.65514	-7	-33	-40
1.6	600	0.95974	-69	-83	0.96104	27	-55	-70
	900	0.95082	-50	-68	0.95273	16	-35	-55
	1,200	0.94283	-29	-53	0.94579	15	-30	-56
2.4	600	1.09801	-57	-78	1.09919	32	-68	-91
	900	1.08771	-44	-71	1.08980	4	-60	-89
	1,200	1.07879	-40	-73	1.08239	14	-26	-60
3.1	600	1.17592	-63	-88	1.17731	35	-58	-85
	900	1.16511	-72	-104	1.16757	26	-33	-67
	1,200	1.15543	-63	-102	1.15930	-9	-45	-86
3.9	600	1.23842	-77	-106	1.23993	32	-62	-94
	900	1.22733	-60	-96	1.22972	29	-35	-74
	1,200	1.21746	-73	-117	1.22111	-22	-64	-109
4.5	600	1.27378	-84	-117	1.27550	51	-49	-84
	900	1.26232	-53	-93	1.26524	-2	-48	-90
	1,200	1.25243	-56	-103	1.25653	-10	-44	-93
5.0	600	1.29829	-68	-103	1.29969	35	-64	-101
	900	1.28659	-74	-117	1.28937	11	-52	-97
	1200	1.27637	-57	-106	1.28053	-28	-61	-112

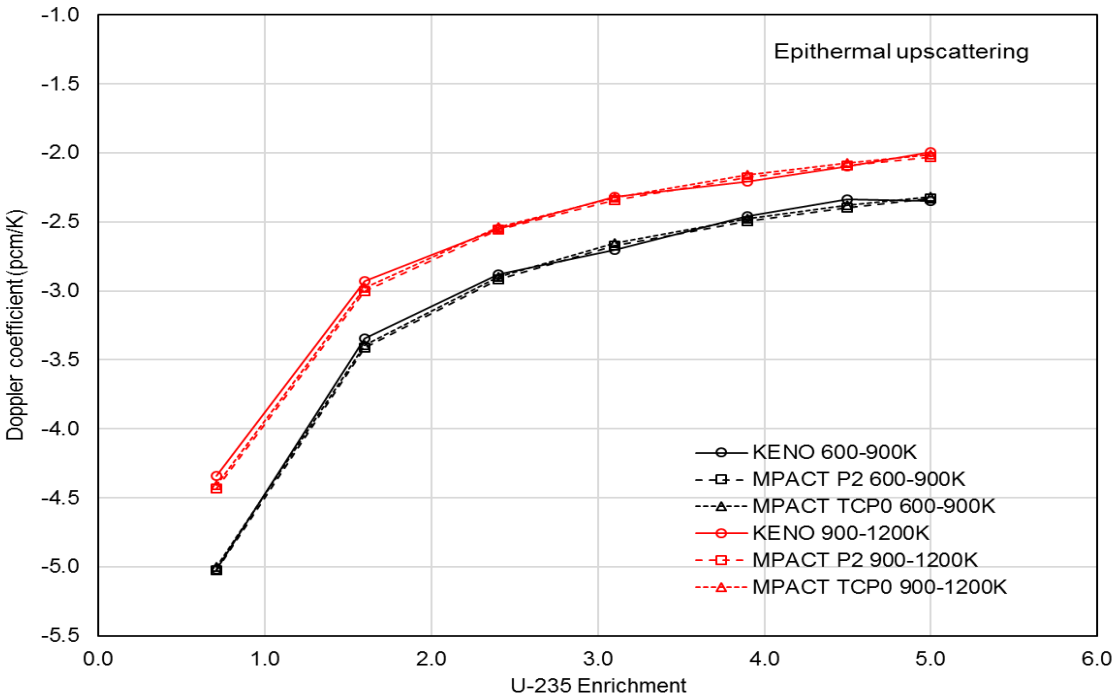

Figure 4.19. Comparison of Reactivities for the Nonuniform Temperature Distributions with Epithermal Upscattering.

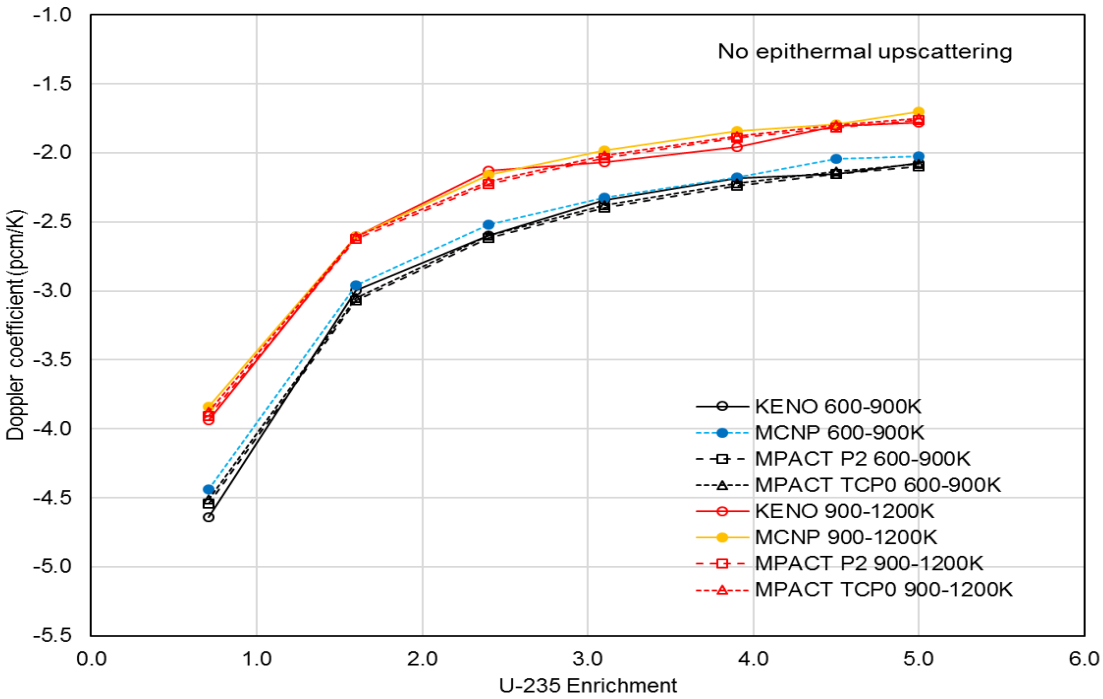

Figure 4.20 Comparison of Reactivities for the Nonuniform Temperature Distributions without Epithermal Upscattering.

5 CONCLUSIONS AND FUTURE WORK

The ENDF/B-VII.1 v4.3m1 MPACT 51-group library has been successfully developed through verification and validation to meet VERA-CS SQA requirements and to satisfy accuracy requirements. Currently, the default cross section library for MPACT is the v4.2m5 ENDF/B-7.1 MPACT 51-g library. To overcome some of drawbacks of the default MPACT MG library, a new MPACT MG library has been developed. Table 5.1 provides the information for the ENDF/B-VII.1 v4.3m1 MPACT 51-group library.

Table 5.1. v4.3m1 MPACT 51-Group Library

Description	File Name
ENDF/B-7.1 MPACT 51-g library	mpact51g_71_4.3m1_sph01.fmt
	2018.2.1 15:45
	404160a90a4837c6b582d72a2ba0b884

Below are new features of the ENDF/B-VII.1 v4.3m1 MPACT 51-group library compared to the current default library, ENDF/B-VII.1 v4.2m5 MPACT 51-g library.

a. Improvement of ^{238}U resonance data based on new CE KENO,
b. ^{135m}Xe (54735) cross sections from TENDL,
c. Temperature-dependent ^{135}Xe cross sections,
d. No fuel temperature reactivity bias,
e. Improvement of ^{167}Er thermal resonance cross sections,
f. 2 new effective cross sections of ^{103}Rh (45001 and 45002) for the rhodium detector,
g. Improvement of ^{155}Gd and ^{157}Gd cross sections,
h. Improvement of ^{107}Ag and ^{109}Ag cross sections, and
i. New ^{124}Sb (51124) and ^{125}Sb (51125) cross section for the Sb-Be secondary neutron source.

REFERENCES

[Bec10] B. Becker, *On the influence of the Resonance Scattering Treatment in Monte Carlo Codes on High Temperature Reactor Characteristics*," PhD Thesis, University Stuttgart (June 2010).

[CAS15] *Consortium for Advanced Simulation of Light Water Reactors (CASL)*. http://www.casl.gov/ (2015).

[Cho02] J. Y. Cho, H. G. Joo, Kang Seog Kim, and S. Q. Zee, "Cell Based CMFD Formulation for Acceleration of Whole-core Method of Characteristics Calculation," *Journal of the Korean Nuclear Society*, 34, **3**, 250–258 (2002).

[Cul74] Dermott E. Cullen, "Application of the Probability Table Method to Multigroup Calculations of Neutron Transport," *Nucl. Sci. Eng.*, **55**, 387–400 (1974).

[Gen17] C. Gentry, A. T. Godfrey, and F. Franceschini, " AP1000® Benchmarking of VERA Neutronics Toolset," *M&C 2017* (Submitted).

[Gol62] R. Goldstein and E. R. Cohen, "Theory of Resonance Absorption of Neutrons," *Nucl. Sci. Eng*., **13**, 132 (1962).

[God14] A. T. Godfrey, *VERA Core Physics Benchmark Progression Problem Specifications*, CASL-U-2012-0131-004, Rev. 4 (2014).

[God15] A. T. Godfrey et al., *VERA Benchmarking Results for Watts Bar Nuclear Plant Unit 1 Cycles 1-12*, CASL-U-2015-0206-000, Rev. 0 (2015).

[Her13] B. R. Herman, B. Forget, and K. Smith, "Improved Diffusion Coefficients Generated from Monte Carlo Codes," *M&C 2013*, Sun Valley, Idaho, May 5–9, 2013.

[Jam99] M. F. James, "Energy Release in Fission of Th-232, U-233, U-234, U-236, Np-237, Pu-238, Pu-240 and Pu-242," *J. Nucl. Energy*, **23**, 1999.

[Joo09] H. G. Joo and et al., "Subgroup Weight Generation Based on Shielded Pin-Cell Cross Section Conservation," *Ann. Nucl. Energ.*, **36**, 859 (2009).

[Joo05] H. G. Joo, B. S. Han, C. H. Kim, and K. S. Kim, "Implementation of Subgroup Method in Direct Whole Core Transport Calculation Involving Nonuniform Temperature Distribution," *M&C 2005*, Avignon, France, Sept. 12–15, 2005.

[Jun13] Y. S. Jung, C. B. Shim, C. H. Lim, and H. G. Joo, "Practical numerical reactor employing direct whole core neutron transport and subchannel thermal/hydraulic solvers," *Ann. Nucl. Energ.*, **62**, 357–374 (2013).

[Kim15] K. S. Kim, *Procedure to Generate the MPACT Multigroup Library*, CASL-U-2015-1013-000, ORNL/TM-2016/52 (2015).

[Kim18] K. S. Kim, M. L. Williams, A. Holcomb, D. Wiarda, B. K. Jeon, and W. S. Yang, "The AMPX/SCALE Multigroup Cross Section Processing for Fast Reactor Analysis," *PHYSOR 2018*, Cancun, Mexico (2018).

[Kim03] K. S. Kim et al., "Monte Carlo Resonance Treatment for the Deterministic Transport Lattice Codes," *Journal of the Korean Nuclear Society*, **35**, No.6, 581–595 (2003).

[Kim12] K. S. Kim and M. L. Williams, "The Method of Characteristics For 2-D Multigroup and Pointwise Transport Calculation in SCALE/CENTRM," *PHYSOR 2012*, Knoxville, Tennessee, USA, April 15–20, 2012.

[Kim16a] K. S. Kim, *Specification for the VERA Depletion Benchmark Suite*, CASL-U-2015-1014-000, Rev. 0, ORNL/TM-2016/53 (2016).

[Kim16b] K. S. Kim, M. L. Williams, and D. Wiarda, *Investigation of Neutron Leakage Conservation Method to Generate ^{1}H Transport Correction Factors*, CASL-U-2016-1163-000, ORNL/TM-2016/266 (2016).

[Kim16c] K. S. Kim, *SUBGR: A Program to Generate Subgroup Data for the Subgroup Resonance Self-Shielding Calculation*, CASL-U-2016-1070-000 (2016).

[Kha71] A. Khairallah and J. Recolin, "Calcul de l'autoprotection résonnante dans les cellules complexes par la méthode des sous-groupes," *Proc. Seminar IAEA-SM-154 on Numerical Reactor Calculations*, 305–317, IAEA, Vienna (1972).

[Lee11] C. H. Lee and W. S. Yang, *MC^2-3: Multigroup Cross Section Generation Code for Fast Reactor Analysis*, ANL-NE-11-41, Argonne National Laboratory (2011).

[Lee09] D. J. Lee, K. Smith, and J. Rhodes, "The Impact of ^{238}U Resonance Elastic Scattering Approximations on Thermal Reactor Doppler Reactivity," *Ann. Nucl. Energy*, **36**, 274–280 (2009).

[Les87] F. Leszczynski, "Neutron Resonance Treatment with Details in Space and Energy for Pin Cells and Rod Clusters," *Ann. Nucl. Energy*, **14**, 589–601 (1987).

[Liu16a] Y. Liu, *Reaction Rate Analysis for MPACT Cross Section Library Verification*, CASL-U-2016-1255-000, Rev. 0 (2016).

[Liu16b] Y. Liu, et al., *Runtime Improvements to the Cross Section Calculation in MPACT*, CASL-X-2016-1105-000, May (2016).

[Mac94] R. E. MacFarlane and D. W. Muir, "The NJOY Nuclear Data Processing System Version 91," LA-12740-M Manual (1994).

[Mpa13] *MPACT: User's Manual Version 1.0.0*, November 8, 2013.

[Mos07] R. Mosteller, "The Doppler-Defect Benchmark: Overview and Summary of Results," *M&C+SNA 2007*, Monterey, CA, April 15-19, 2007.

[Pal17a] S. Palmtag, *MPACT Library Verification by Comparison of Pincell Calculations to Monte Carlo Results*, CASL-U-2016-0281-002, Rev. 2 (2017).

[Pal16b] S. Palmtag, *MPACT Library Verification by Comparison of Assembly Calculations to Monte Carlo Results*, CASL-U-2016-1052-001, Rev. 0 (2017).

[Ryu14] M. R. et al., "Incorporation of Anisotropic Scattering in nTRACER," *Transaction of the Korean Nuclear Society Autumn Meeting*, Pyeongchang, Korea, October 30–31, 2014.

[Sca16] *SCALE: A Modular Code System for Performing Standardized Computer Analyses for Licensing Evaluation*, ORNL-TM/2005/39, Version 6.2, ORNL, Oak Ridge, Tennessee, available from Radiation Safety Information Computational Center at Oak Ridge National Laboratory as CCC-834 (2016).

[Sta83] R. J. J. Stamm'ler and M. J. Abbate, *Methods of Steady-State Reactor Physics in Nuclear Design*, Academic Press (1983).

[Sta03] R. J. J. Stamm'ler et al., *The HELIOS Methods*, Studsvik Scandpower (2003).

[Tur16] J. Turner et al., "The Virtual Environment for Reactor Applications (VERA): Design and architecture," *Journal of Computational Physics*, **326**, 544 (2016).

[Wia16] D. Wiarda, M.E. Dunn, N.M. Green, M. L. Williams, C. Celik and L. M. Petrie, *AMPX-6: A Modular Code System for Processing ENDF/B*, ORNL/TM-2016/43 (2016).

[Wem07] C. A. Wemple, et al., "Improved Temperature-Dependent Resonance Treatment in HELIOS-1.9," *Trans. Am. Nucl. Soc.*, **96**, 657–659 (2007).

[Wil12] M. L. Williams and K. S. Kim, "The Embedded Self-Shielding Method," *PHYSOR 2012*, Knoxville, Tennessee, USA, April 15–20, 2012.

[Wil06] M. L. Williams, M. Asgari, and D. F. Hollenbach, *CENTRM: A One-Dimensional Neutron Transport Code for Computing Pointwise Energy Spectra*, ORNL/TM-2005/39, Version 5.1, Vol. II, Book 4, Sect. F18 (2006).